UNIVERSITY OF TARTU
Faculty of Science and Technology
Institute of Chemistry

Wiljar Lobjakas

Platinum catalysts deposited onto peat-derived carbon for oxygen reduction reaction in a proton-exchange membrane fuel cell

Master's Thesis (30 ECTS)
Curriculum: Materials and Processes for Sustainable Energetics

Supervisors: Jaak Nerut, PhD
Heili Kasuk, PhD

Tartu 2023

Infoleht

Turbast sünteesitud süsinikule sadestatud plaatinakatalüsaatorid hapniku redutseerimiseks prootonvahetusmembraaniga kütuseelemendis

Käesolevas töös uuriti hapniku redutseerimise reaktsiooni (ORR) turbast sünteesitud süsinikalusmaterjalile sadestatud plaatinakatalüsaatoritel. Katalüsaatormaterjale sünteesiti mitme erineva sünteesi meetodiga. Uuritavate materjalide füüsikaliseks karakteriseerimiseks teostati osakese suuruse mõõtmised, N_2 sorptsioonianalüüs, röntgenstruktuurianalüüs, termogravimeetriline analüüs ja skaneeriv elektronmikroskoopia energiat hajutava röntgenspektroskoopiaga. Elektrokeemiliseks karakteriseerimiseks mõõdeti materjalide elektrokeemiliselt aktiivne pindala kolmeelektroodse süsteemiga 0,1 M $HClO_4$ lahuses ja prootonvahetusmembraaniga kütuseelemendi (PEMFC) ühikrakus. Materjalide ORR-i kineetikat uuriti pöörleva ketaselektroodi meetodiga. PEMFC ühikrakus uuriti materjalide aktiivsust. Saadud andmeid võrreldi kommertsiaalse katalüsaatormaterjali (60% Pt on Ketjenblack EC-300J) tulemustega.

Märksõnad: hapniku redutseerimise reaktsioon, PEMFC, plaatina, turbasüsinik, katalüsaatori alusmaterjal

CERCS: T140 Energeetika, T152 Komposiitmaterjalid, P401 Elektrokeemia

Platinum catalysts deposited onto peat-derived carbon for oxygen reduction reaction in a proton-exchange membrane fuel cell

The aim of this thesis was to investigate the oxygen reduction reaction on platinum catalysts deposited onto peat-derived carbon. Catalyst materials were synthesised using several different methods. Physical characterisation of the materials was carried out through particle size measurements, N_2 sorption analysis, X-ray diffraction analysis, thermogravimetric analysis, and scanning electron microscopy with energy-dispersive X-ray spectroscopy. Electrochemical characterisation was done by measuring the electrochemically active surface area of the materials using a three-electrode system in 0.1 M $HClO_4$ solution and a proton-exchange membrane fuel cell (PEMFC) single cell. The ORR kinetics of the materials were investigated using a rotating disc electrode method. The activity of the materials was also tested in a PEMFC single cell. The obtained data were compared with the results of a commercial catalyst material (60% Pt on Ketjenblack EC-300J).

Keywords: oxygen reduction reaction, PEMFC, platinum, peat-derived carbon, catalyst support

CERCS: T140 Energy research, T152 Composite materials, P401 Electrochemistry

Table of contents

Abbreviations

ads/des – adsorption and desorption

CNF – carbon nanofibers

CNT – carbon nanotubes

CV – cyclic voltammetry

ECSA – electrochemically active surface area

EIS – electrochemical impedance spectroscopy

EDL – electrical double-layer

GDL – gas diffusion layer

HOR – hydrogen oxidation reaction

K-L – Koutecky-Levich

MA – mass activity

MC – mesoporous carbon

MEA – membrane electrode assembly

MV – mean volume diameter

NPM – non-precious metals

OCV – open-circuit voltage

ORR – oxygen reduction reaction

PDC – peat-derived carbon

PEMFC – proton-exchange membrane fuel cell

RDE – rotating disc electrode

RHE – reversible hydrogen electrode

rpm – revolutions per minute

SA – specific activity

SEM-EDX – scanning electron microscopy with energy dispersive X-ray spectroscopy

TGA – thermogravimetric analysis

XRD – X-ray diffraction

2D-NLDFT-HS – two-dimensional non-local density functional theory

Introduction

Using non-renewable fuels, such as oil, natural gas, coal, etc., for energy production creates unwanted by-products, such as CO_2. The European Union and Estonia aim to reduce CO_2 emissions by 55% by 2030 and achieve carbon neutrality by 2050 [1]. This creates a need to significantly accelerate the development and implementation of green technologies. Hydrogen, which contributes to the green transition as a storage option, has been among the most important proposed solutions lately. A way to replace energy production from fossil fuels and do it without generating pollutants is to produce energy from hydrogen using fuel cells [2–4].

A fuel cell is an electrochemical energy conversion device that directly converts the chemical energy of fuel into electrical energy. One of the many types of fuel cells is the proton-exchange membrane fuel cell (PEMFC), which uses oxygen (air) and hydrogen to produce energy. PEMFC is an energy production device with high efficiency and no pollutants (produces electricity, water, and heat) [2–4]. At the cathode of the PEMFC, the oxygen reduction reaction (ORR) occurs, which is relatively slow compared to the hydrogen oxidation reaction (HOR) occurring at the anode [5]. Catalysts are used to accelerate the ORR process. Generally, catalysts are based on precious metals, such as platinum [3–6]. The catalyst support material, which affects both the stability and activity of the catalyst, is also very important [7].

The objectives of this thesis are:

1. Synthesis of platinum catalyst materials, which involves the processing of carbon support material synthesised from peat and deposition of Pt onto the support material.
2. Inquiry of support and catalyst materials using physical characterisation methods: determination of particle size using light diffraction, low-temperature N_2 sorption, X-ray diffraction analysis (XRD), thermogravimetric analysis (TGA), and scanning electron microscopy with energy dispersive X-ray spectroscopy (SEM-EDX).
3. Determination of the activity of synthesised catalysts using the rotating disc electrode method (RDE).
4. Optimisation of the catalyst layer coating method and to utilise the synthesised catalysts in a PEMFC.

The properties of the synthesised catalysts were compared to a commercial catalyst.

The main focus of the work is on developing support materials synthesised from peat and developing Pt deposition methods onto carbon support materials. The possibility of adding value to Estonian raw materials was also investigated since the peat used was from Möllatsi, an Estonian deposit.

1. Literature overview

1.1. Fuel cells

A fuel cell is an electrochemical energy conversion device that converts the chemical energy of the fuel into electrical energy. Each fuel cell has three main parts: a cathode, an anode, and an electrolyte in between, and the electrodes are connected to an external circuit. The electrodes are constantly supplied with reactants necessary for the reactions taking place there. At the anode, hydrogen (or another fuel such as methanol) is oxidized, while at the cathode, oxygen is reduced. The electrolyte between the electrodes is ion-conductive. Depending on the type of fuel cell, the electrolyte can conduct either anions (O_2^-, OH^-, CO_3^{2-}) or protons (H^+). Fuel cells come in different types and are mainly classified based on the choice of electrolyte, fuel, or operating parameters (such as temperature). The most popular types of fuel cells and their parameters are described in Table 1. [2–4]

Table 1. Comparison of different types of fuel cells [3,4].

Fuel cell	Fuel	Temperature range	Electrolyte	Moving ions	Catalyst
Proton-exchange membrane fuel cell	H_2	60–100 °C	Nafion	H^+	Pt
Solid oxide fuel cell	CH_4	700–1000 °C	Y_2O_3, ZrO_2	O^{2-}	$CaTiO_3$
Direct methanol fuel cell	CH_3OH	60–200 °C	Solid polymer	H^+	Pt
Alkaline fuel cell	H_2	150–250 °C	KOH	OH^-	Pt
Molten carbonate fuel cell	CH_4	500–700 °C	$(NaK)_2CO_3$	CO_3^{2-}	Ni
Phosphoric acid fuel cell	H_2	150–250 °C	H_3PO_4	H^+	Pt

Different types of fuel cells are used for various applications. PEMFCs are commonly used in vehicles because they operate at low temperatures and can start up quickly. Direct methanol fuel cells are also used in portable devices and small-scale applications. Solid oxide fuel cells, phosphoric acid fuel cells, and molten carbonate fuel cells are often used in large buildings or industrial settings because they are reliable, operate at high temperatures, and can handle impurities in the fuel. Alkaline fuel cells were one of the first types of fuel cells to be developed and are still used today in space missions because they are lightweight and can operate with high efficiency in low-pressure environments. [2,4–6]

1.2. Proton-exchange membrane fuel cell

A PEMFC consists of a membrane electrode assembly (MEA). MEA is formed from a polymer electrolyte membrane that conducts protons between two porous and electrically conducting electrodes. Nafion is mainly used as a membrane in PEMFCs. On both sides of the MEA, there are gas diffusion layers (GDLs), gas flow channels (sometimes engraved into the bipolar contact plates), and contact plates. The construction of a single element is shown in Fig. 1. [6,8]

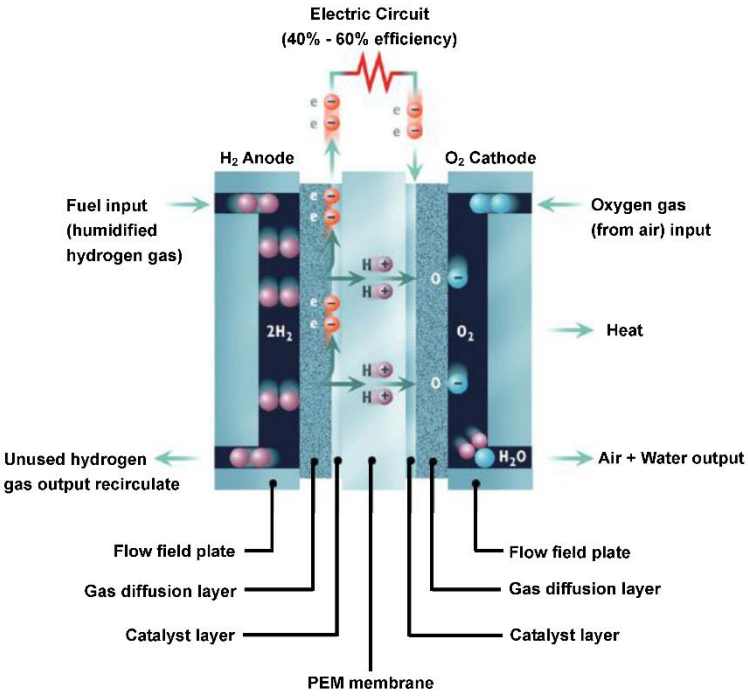

Figure 1. Working principle of a proton-exchange membrane fuel cell [8].

Hydrogen is used as fuel, which is directed to the anode where hydrogen is oxidized into protons (Eq. 1). The protons move through the proton exchange membrane to the cathode, and the released electrons move to the other side of the membrane through an external circuit. At the cathode, with oxygen directed to it and protons coming through the membrane, ORR occurs, producing water (Eq. 2). As a result of the processes in the fuel cell, heat is released, and electrical energy and water are produced. Catalysts are used on both electrodes to accelerate the half-reactions. In practical applications, the catalyst is usually Pt on a carbon support material. The catalyst layer is located between the GDL and the polymer membrane. Both the cathode and anode reactions occur simultaneously in the fuel cell (overall chemical equation: $2H_2 + O_2 = 2H_2O$). The equations describing the half-reactions taking place in the unit cell are:

$$\text{Anode: } 2H_2 \rightarrow 4H^+ + 4e^- \quad (1)$$

$$\text{Cathode: } O_2 + 4H^+ + 4e^- \rightarrow 2H_2O \quad (2)$$

The efficiency of the PEMFC is limited by the cathode's ORR rate because the anode's hydrogen oxidation process is fast compared to the ORR. [3–6]

1.3. Cathode catalysts

Low-temperature fuel cells, such as PEMFC, require highly active catalysts to promote HOR at the anode and ORR at the cathode. It is particularly important to use an active catalyst to accelerate the ORR at the cathode because ORR is relatively slow compared to the HOR occurring at the anode [5]. Precious metals and non-precious metals (NPMs) are used as cathode catalysts. NPMs include nickel, iron, cobalt, chromium, copper, tungsten, tin, etc. All of these metals are active in catalysing ORR [9,10]. The main problem with NPM catalysts is their durability. Compared to precious metal catalysts, NPM catalysts degrade faster, resulting in a decrease in catalytic activity. Among precious metals, platinum has shown the highest electrocatalytic activity in ORR catalysing. Other precious metals, such as palladium and ruthenium, as well as various alloys, have also been investigated as ORR catalysts. Pd and Ru have physical and chemical properties similar to platinum. Nevertheless, Pd and Ru show lower electrocatalytic activity than Pt. This is why Pt and its alloys are the most widely used ORR catalyst compared to other catalysts. [9,11]

1.4. Carbon catalyst supports

Since the price of precious metals is high and their quantity is limited, research is also being conducted on catalyst support materials to achieve better dispersion of catalytically active material. The catalyst support materials affect the price, activity, and durability of PEMFCs. Good electrical conductivity, high surface area, porous structure, corrosion resistance, and water transport capability are essential parameters for catalyst support materials. These properties ensure high catalytic activity, stability, durability, and optimal mass transfer, reducing the catalyst cost [7]. Carbon materials with a high surface area are the most commonly used catalyst supports in low-temperature fuel cells. Carbon support materials should be predominantly mesoporous (pore size 20-40 nm) to ensure high surface area, thus providing a good connection between the catalyst nanoparticles and the electrolyte ionomers. A large surface area (greater than 100 $m^2 g^{-1}$) is necessary to ensure uniform distribution of Pt nanoparticles. The support material must also be electrochemically stable under fuel cell operating conditions. [12,13]

Carbon materials are widely used as catalyst support materials in PEMFCs. For example, commercial catalyst materials use carbon black, such as Vulcan XC-72 or Ketjenblack EC-300J, which have good electrical conductivity and high surface area. In addition to carbon black, there are other carbon materials used as catalyst supports in PEMFCs, including

mesoporous carbons (MC) (pore size 2-50 nm), carbon nanotubes (CNT), carbon nanofibers (CNF), etc. [12,13]. Compared to carbon black, MC materials have a larger surface area and fewer micropores. These properties promote the even distribution of Pt catalyst nanoparticles, resulting in high surface area and catalytic activity. The mesoporous structure of the support material also facilitates smooth mass transport, providing high current values limited by mass transfer. More graphite-like support materials, as CNT and CNF, are usually more stable than other carbon supports, because carbon corrosion occurs slowly in these materials. [12–14]

Carbon materials have also been synthesised from natural carbohydrates such as peat, sugar (plant-based sucrose), trees (cellulose), coffee beans, and others [15]. In this thesis, the carbon support material for the Pt catalyst was synthesised from highly decomposed peat. The chemical properties of peat include mostly organic components (C, H, O, N, S), but it also includes inorganic components (Si, Fe, Al, Ca, Mg). The elemental proportion of lowly decomposed peat resembles that of wood, while highly decomposed peat approximates that of lignite (brown coal) [16]. Peat-derived carbons (PDCs) have been used as electrode materials for high-efficient electrical double-layer (EDL) capacitors [17]. N_2 sorption measurement results show that these carbon materials are mainly microporous but also contain a reasonable amount of smaller mesopores and have a high specific surface area, up to $S_{BET} = 2150\ m^2\ g^{-1}$. PDCs have also been studied as hard carbon electrodes with superior capacity for sodium-ion batteries, non-platinum group metal oxygen electrocatalysts, and fuel cell cathodes [18,19].

1.5. Rotating disc electrode method

The RDE method is used to study electrochemical reactions, including the kinetics of ORR. The RDE method is used to determine the initial activity of catalysts, which allows for the selection of suitable catalysts for single-cell experiments. [20]

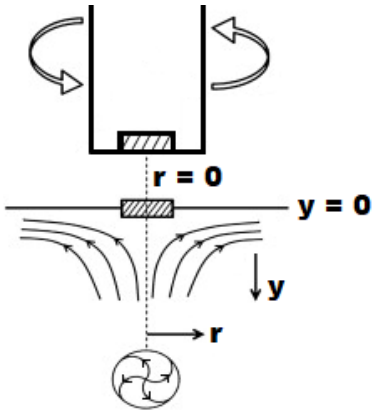

Figure 2. Movement of the solution under a rotating disc electrode. [19].

The main component of the RDE method is a working electrode, such as a glassy carbon disc electrode, which is rotated by the rotator in an electrolyte solution [21]. Due to the rotation of the disc electrode, the electrolyte solution begins to move uniformly (Fig. 2), and the movement velocity depends on the distance from the electrode surface. The movement of particles in the solution can occur in three ways: diffusion, convection, and migration. [22,23] One of the most important characteristics of the RDE method is that the flow rate of the

electrolyte solution is laminar. Due to this property, it is possible to calculate the mass transport rate using the Levich equation. For ORR, the diffusion-limited current density, j_d, can be found using the formula [24]:

$$j_d = -0.62\, n\, F\, D_{O_2}^{2/3}\, \omega^{1/2}\, \nu^{-1/6}\, c_{O_2}\,, \tag{3}$$

where, n, is the number of electrons transferred for each oxygen molecule, F, is the Faraday constant (96485 C mol^{-1}), D_{O_2}, is the diffusion coefficient of oxygen (1.93×10^{-5} cm^2 s^{-1}), $\omega = 2\pi f$, is the angular rotation rate of the electrode, f, is the rotation rate of the electrode (rpm, revolutions per minute), ν, is the kinematic viscosity of the solution (1.009×10^{-2} cm^2 s^{-1}) and, c_{O_2}, is the oxygen concentration in the solution (1.26×10^{-3} mol dm^{-3}). The values in parentheses are valid for a 0.1 M $HClO_4$ solution at a temperature of 25 °C [25]. The oxygen diffusion-limited current density for a four-electron process (n = 4) is 59.8 A m^{-2} at an electrode rotation rate of 1 600 rpm [25].

In the case of mixed kinetics, the Koutecky-Levich equation (K-L) can be applied to determine the kinetic current density, j_{kin}, from the total current density, j:

$$\frac{1}{j} = \frac{1}{j_{kin}} + \frac{1}{j_d} = \frac{1}{-n\, F\, k\, c} + \frac{1}{-B\, \omega^{1/2}}\,, \tag{4}$$

where, k, is the rate constant for ORR and, $B = 0.62\, n\, F\, D_{O_2}^{2/3}\, \nu^{-1/6}\, c_{O_2}$ [24,25].

Fig. 3 shows the current density dependence of oxygen reduction on potential (RDE experiment), with three distinct regions visible. In the area of charge transfer (green), the limiting stage of the overall reaction is the slow charge transfer. In this area, the current values increase exponentially with increasing overpotential. In the mass transfer region (gray), the current density depends on the electrode rotation rate (Eq. 3). The limiting step is diffusion, where the concentration gradient influences the mass transfer rate of the substance to the electrode surface. A plateau is formed in the mass transfer region where the current almost does not change when changing the potential. In the mixed kinetics region (blue), the reaction rate is limited by both slow

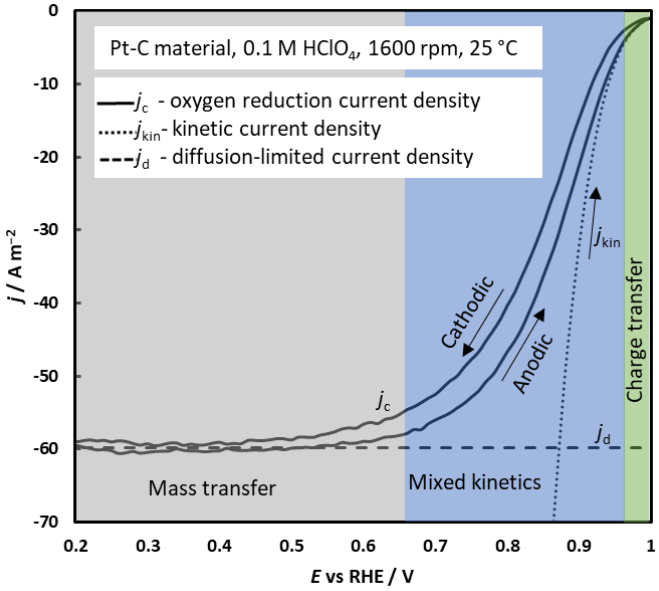

Figure 3. The current density dependence of oxygen reduction on the potential in a rotating disc electrode experiment.

charge transfer and diffusion. Fig. 3 also shows the kinetic current density and the calculated diffusion-limited current density. The region of mixed kinetics corresponds to a current density range of 0.05 j_d...0.95 j_d (3...57 A m^{-2}). [24]

1.6. PEMFC single cell testing

The true activity (under operating conditions) of a PEMFC catalyst can be evaluated by conducting a test with the catalyst in question in an actual PEMFC single cell. The PEMFC single cell activity evaluation utilises a polarization curve, representing the cell voltage as a function of current density (Fig. 4).

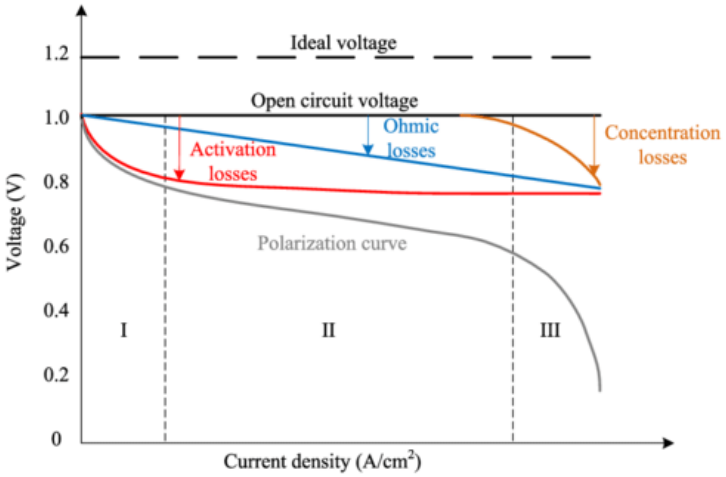

Figure 4. Dependence of PEMFC single cell voltage on current density and main types of overpotential [28].

The single cell's measured open circuit voltage (OCV) is smaller than expected due to hydrogen gas leakage through the membrane. When current is drawn from the PEMFC, its voltage decreases due to kinetic (activation), ohmic (*IR*), and mass transfer (concentration) losses. These types of overpotential are shown on the polarization curve in Fig. 4. Ohmic voltage drop (area II) is caused by the resistance of the single cell components (membrane, GDL, etc.). The causes of ohmic voltage drop have been extensively studied and can be reduced by optimising the membrane and GDL. Kinetic losses (area I) are mainly due to slow ORR and account for the most significant proportion of overpotential. Kinetic overpotential can be reduced by developing more active catalysts. Mass transfer losses (area III) are due to the slow transport of reactants to the reaction centre. Mass transfer losses can be reduced by optimising the structure of GDL and catalyst (porosity). [26–28]

1.7. Electrochemically active surface area

In electrochemistry, ECSA stands for electrochemically active surface area (of platinum nanoparticles). ECSA describes the area of an electrode that is available for electrochemical reactions. That means the surface area of the electrode that is in contact with the electrolyte (solution) and can participate in redox reactions. ECSA can influence the rate and efficiency of reactions on the electrode surface, which is why it is an important parameter in many electrochemical processes. [29]

Fig. 5 shows the dependence of platinum catalyst capacitance on electrode potential, and such graphs are used to calculate platinum ECSA. Capacitance, *C*, values are obtained from the values of current density, *j*, and potential scan rate, *v*, using the formula: C = *j*/*v*. A rectangular area in the figure represents the platinum EDL area. The capacitance is the smallest in the EDL area and is determined by the charging and discharging of the platinum EDL and support material. In the cyclic voltammetry (CV), the hydrogen adsorption/desorption (ads/des) area is observed at cathodic electrode potentials, and the oxygen ads/des area is observed at anodic potentials. In ECSA calculations it is assumed that each surface layer Pt atom adsorbs one hydrogen atom. [24,30]

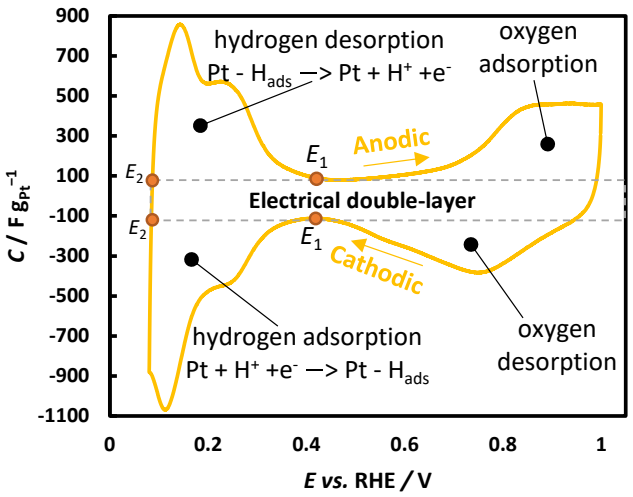

Figure 5. Dependence of the Pt catalyst capacitance on potential.

ECSA is calculated from the formula:

$$\mathrm{ECSA} = \frac{q_{\mathrm{Pt-H}}}{q_{\mathrm{Pt-H,poly}}\, m_{\mathrm{Pt}}}\,, \tag{5}$$

where, m_{Pt}, is the mass (in grams) of platinum on the electrode, $q_{\mathrm{Pt\text{-}H}}$, is the charge for hydrogen ads/des and, $q_{\mathrm{Pt\text{-}H,poly}}$, is the charge required for the formation of a monolayer of adsorbed hydrogen on an ideally smooth Pt surface, which has a value of 210 μC cm^{-2} [30,31]. The charge for hydrogen ads/des, $q_{\mathrm{Pt\text{-}H}}$ (C), can be determined using the formula:

$$q_{\mathrm{Pt-H}} = q - q_{\mathrm{EDL}} \tag{6}$$

The total charge, *q*, was found by integrating *C*,*E*- dependencies:

$$q = \int_{E_1}^{E_2} C\,dE \tag{7}$$

The charge of EDL, q_{EDL}, is calculated from the formula (C_{EDL} = const)

$$q_{\mathrm{EDL}} = \int_{E_1}^{E_2} C_{\mathrm{EDL}}\,dE = C_{\mathrm{EDL}} \int_{E_1}^{E_2} dE = C_{\mathrm{EDL}} E\big|_{E_1}^{E_2} = C_{\mathrm{EDL}}(E_2 - E_1) \tag{8}$$

The capacitance of the EDL is taken from the minimum capacitance |*C*| of the platinum EDL area of the corresponding direction. The potential values from the anodic direction minimums and cathodic direction maximums are used for the paths. E_1 is taken from the platinum EDL area, and E_2 is taken from the hydrogen ads/des area (Fig. 5). [20,24,30,32]

2. Experimental

2.1. Synthesis of carbon support material

Synthesis of the PDC. Highly decomposed peat was collected from a bog in Möllatsi, Estonia. The PDC was prepared in three stages. Firstly, 1 kg of wet peat was dried to obtain 100 g of dry peat. The peat was washed with MilliQ$^+$ water, homogenized, and pre-pyrolysed for 3 hours at 450 °C. 35 g of carbonaceous material was obtained from the dried peat, which was mixed with a 20% KOH solution (prepared from solid KOH (Chemapol, pure)) and heated for 2 hours at 70 °C. Then, a 50% (by volume) HCl solution (Alfa Aesar, Product No.: 35607) was added until the solution pH was approximately 1 (determined with indicator paper), and the solution was stirred overnight with a magnetic stirrer. To remove residues, the carbonaceous material was mixed with MilliQ$^+$ water (resistance at 25 °C is 18.2 MΩ cm^{-1}), washed, filtered, and dried in a vacuum oven (80 mbar, 100 °C). The prepared carbon had a yield of 26 g. In the next step, the carbonaceous material was post-pyrolysed at a temperature of 800 °C. The pre-pyrolysis was carried out in a quartz tube furnace (Carbolite), and the post-pyrolysis was carried out in an Al_2O_3 tube furnace (Carbolite Gero) in an argon environment (5.0, As Linde Gas). From the post-pyrolysis, 19 g of material was obtained. This synthesis was conducted twice, so two batches of PDC were obtained: **PDC1** and **PDC2**. The PDC synthesis was performed by Anu Adamson. [18]

Milling and H_2 reduction of the PDC. The first batch, **PDC1**, was wet-ground in a zirconium oxide (ZrO_2) crucible with 1 cm in diameter yttria-stabilized zirconia balls (Inframat, Advanced Materials 5.3 wt% Y_2O_3), MilliQ$^+$ water, and isopropyl alcohol (J. T. Baker, 99.5%) was added. Planetary ball milling was performed using a FRITSCH Pulverisette 6 at a speed of 350 rpm for 2 hours (rotation direction switched in every 15 min) to achieve the desired particle size**.** After milling, the carbon material was vacuum filtered. The filtrate was dried overnight in a vacuum drying oven (memmert VO 400) at a pressure of 50 mbar and a temperature of 80 °C. During grinding, zirconia could entere the carbon material from the crucible and balls. Then, the functional groups (-OH, -COOH, -CHO, etc.) in the carbon material were reduced with hydrogen. The carbon material was placed in a furnace (Carbolite CTF 12/65/550) and heated with a flow of argon (5.0, AsLinde Gas) to a temperature of 800 °C. At this temperature, the carbon material was reduced with a flow of hydrogen (6.0, Model NMH2 500, As Linde Gas) for 2 hours. Finally, the carbon material was manually ground for 30 minutes in a corundum crucible. The second batch, **PDC2**, was only wet-ground and was not reduced with H_2. Smaller, 1 mm in diameter yttria-stabilized zirconia balls (Inframat, Advanced Materials 5.3 wt% Y_2O_3)

were used. The material was milled for 4 hours, and particle size was determined after each hour. The carbons produced were labeled **PDC1**(2h milled, 2h H_2) and **PDC2**(4h milled).

2.2. Synthesis of the catalysts

In the synthesis of platinum catalysts, platinum complex ($H_2PtCl_6{\times}6H_2O$, Alfa Aesar, 99.9%, metals basis) was used as a source for platinum. The chloroplatinic acid was reduced by isopropyl alcohol, sodium borohydride [33,34], or ethylene glycol (Lach-Ner, 99.98%) [34–39]. The desired Pt percentage by weight in the catalyst material was approximately 60%. Materials **IPA**, **NBH**, **EG1**, **EG2**, **EG3**, and **EG4** were synthesised. Fig. 6 shows a scheme to describe the synthesis of the catalyst materials.

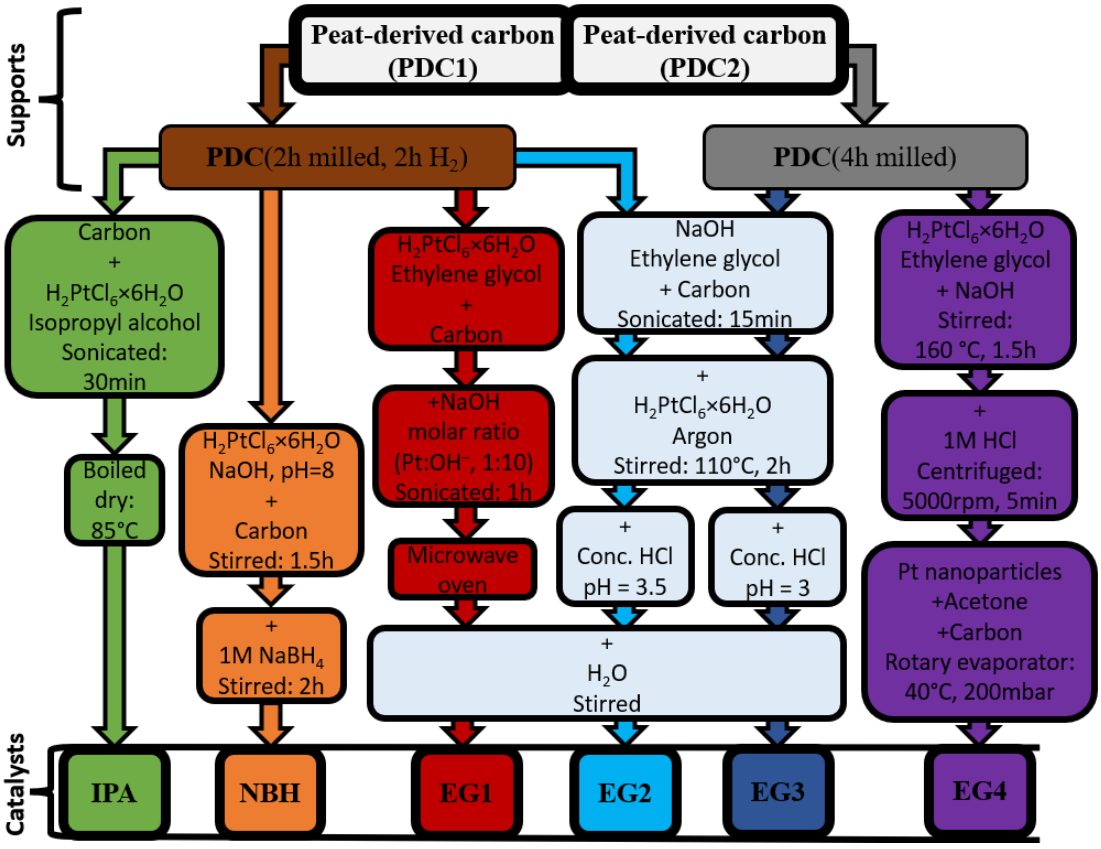

Figure 6. A scheme to describe the synthesis of the catalyst materials.

Isopropyl alcohol reduction method. The Pt-nanoparticles were deposited onto the carbon support for the **IPA** catalyst material by the isopropyl alcohol reduction method. 803 mg of $H_2PtCl_6{\times}6H_2O$ was added to 12 cm^3 of isopropyl alcohol (J. T. Baker, 99.5%). The mixture was sonicated in an ultrasonic bath Elmasonic P 30 H (Elma) for 1 min (37 kHz, 100%). The previously prepared Pt-compound mixture was added to 201 mg of **PDC1**(2h milled, 2h H_2) in three portions of 4 cm^3. After adding each portion, the mixture was sonicated for 30 min, then dried in an oven at 85 °C until the isopropyl alcohol had evaporated.

Sodium borohydride reduction method. For the **NBH** catalyst material, the Pt-nanoparticles were deposited onto the carbon support using the sodium borohydride reduction method [33,34]. The required amount of 804 mg of $H_2PtCl_6 \times 6H_2O$ was dissolved in 1500 cm^3 of $MilliQ^+$ water to prepare a solution with a Pt-compound concentration of ~1 mM. The prepared solution was stirred at room temperature for 45 min. 20 wt% NaOH was added until the pH of the solution reached ~8. 204 mg of **PDC1**(2h milled, 2h H_2) was added to the Pt-solution. After that, 1 M $NaBH_4$ solution was prepared by dissolving 1.164 g of $NaBH_4$ (Aldrich Chemistry, 98.0%) in 30.8 cm^3 of $MilliQ^+$ water. The prepared 1 M $NaBH_4$ solution was added dropwise to the previously prepared Pt and carbon suspension. The reaction mixture was stirred for 2 h and left to settle overnight. The catalyst was filtered, rinsed, and dried in a vacuum oven at 50 mbar and 110 °C.

Microwave-assisted ethylene glycol reduction method. For the **EG1** catalyst material, the Pt-nanoparticles were deposited onto the carbon support by the microwave-assisted ethylene glycol reduction method [34,35]. 807 mg of $H_2PtCl_6 \times 6H_2O$ was dissolved in 1 cm^3 of $MilliQ^+$ water, 201 mg of **PDC1**(2h milled, 2h H_2) was also added to the mixture. Then, 60 cm^3 of ethylene glycol was added, and the pH was regulated by adding 20 wt% NaOH ($Pt:OH^-$ molar ratio was 1:10). The mixture was sonicated for 1 h. The suspension was heated using a commercial 750 W microwave for 80 s. After cooling, 500 cm^3 of $MilliQ^+$ water was added. The mixture was stirred overnight. The catalyst prepared was filtered, rinsed, and dried in a vacuum oven at 50 mbar and 100 °C.

Ethylene glycol reduction method using refluxing. For the synthesis of **EG2** and **EG3** catalyst materials, the Pt-nanoparticles were deposited onto the carbon support by ethylene glycol reduction method [36,37]. For the synthesis of **EG2** material, the NaOH aqueous solution was prepared in a reaction flask (Pt:Na molar ratio was 1:10). Then 85 cm^3 of ethylene glycol was added to the flask with 0.169 g of **PDC1**(2h milled, 2h H_2). The mixture was sonicated for 15 min. The synthesis mixture was stirred, and the reaction environment was purged with argon gas (99.999%, As Linde Gas). Then, 0.673 g of a platinum complex was dissolved in 5 cm^3 of $MilliQ^+$ water. The Pt-solution was added to the reaction mixture over 20 min time. The reaction mixture was heated for 2 h at 110 °C in an oil bath. At the same time, the reaction mixture was stirred, and argon in the reaction environment was maintained. After cooling, 0.86 cm^3 of a concentrated HCl solution (purity ≥ 37%, Sigma-Aldrich) diluted in 15 cm^3 of $MilliQ^+$ water was added to the mixture (to achieve pH = 3.5). The mixture was stirred for an additional 20 min and then filtered. The product was dried in a vacuum drying cabinet for 24 hours (100 °C, 50 mbar).

For the **EG3** synthesis the **PDC2**(4h milled) was used as the carbon support material. Also, ethylene glycol and water were added 10% more in volume, and the HCl aqueous solution was added until pH = 3 was achieved.

For PEMFC single cell measurement, adding commercial carbon materials like CNT or Ketjenblack EC-300J carbon black to a synthesised catalyst was tested with **EG3** material [40–42]. The ratio of catalyst to additive carbon was 70% **EG3** and 30% CNT (Aldrich, Carbon nanotubes multi-walled, >90%, outside diameter 10-15 nm, internal diameter 2-6 nm, length 0.1-10 μm, S_{BET} = 280-350 $m^2\ g^{-1}$) or 30% Ketjenblack EC-300J (FuelCellStore, SKU: 6211786). The additives were added during the catalyst ink suspension preparation step. In this case, the following notations were used **EG3 + NT** and **EG3 + KB**, respectively.

Synthesis of Pt nanoparticles separately via ethylene glycol reduction method and deposition onto carbon support. For the synthesis of **EG4** catalyst material, the Pt-nanoparticles were synthesised and collected separately from the carbon. Only after the synthesis of Pt-nanoparticles were they deposited onto the carbon support from suspension in acetone [38,39]. To obtain a colloidal suspension of 2 nm Pt-nanoparticles 9.8 cm^3 of 0.4 M NaOH in ethylene glycol and 9.8 cm^3 40 mM $H_2PtCl_6{\times}6H_2O$ in ethylene glycol were mixed. The mixture was heated in a preheated oil bath at 160 °C for 1.5 h with slow stirring. 1 M HCl solution was added to the dark reaction mixture to deposit and wash the Pt-nanoparticles in a centrifuge (Domel, Centric 250). The nanoparticles were centrifuged (5000 rpm, 5 min) in 1 M HCl solution three times. The nanoparticle residue was stuck to the centrifuge tube, and the HCl solution was poured off. The Pt-nanoparticles were re-dispersed in 18 cm^3 of acetone (OKKO Products, Acetone, purity min. 99.5%). Also, 0.051 g of **PDC2**(4h milled) was dispersed in acetone. Both acetone dispersions were mixed, and the acetone was evaporated in a rotary evaporator (Butchi rotary evaporator assembly) at 40 °C and at 200 mbar until completely dried. The rotary evaporator assembly was made out of a rotavapor R-215, a heating bath B-491, a vacuum pump V-710, and a vacuum controller V-855. The obtained catalyst was dried in a vacuum drying cabinet overnight (100 °C, 50 mbar). Next day, $MilliQ^+$ water was added, and the suspension was sonicated in an ultrasonic bath (0 °C, 35 kHz, 160 W) for 3 min. The material was vacuum filtered and dried in a vacuum drying cabinet (100 °C, 50 mbar).

2.3. Methods of structural characterisation

Particle size analysis. A MICROTRAC S3500 Model Bluewave particle size analyser was used for particle size distribution analysis via dynamic light scattering method [43]. Isopropyl

alcohol was used as a solvent for PDC. For better dispersion, the carbon materials were sonicated in isopropyl alcohol before the procedure for 30 min.

N_2 sorption method. The materials' porosity and specific surface area were evaluated with a Micromeritics ASAP 2020 instrument using the low-temperature (−195.8 °C) N_2 sorption method. The adsorption isotherms were analysed using SAIEUS software, using a two-dimensional non-local density functional theory (2D-NLDFT) [44,45]. The theory assumes that the adsorbing surface is energetically and structurally heterogeneous. The specific surface area (S_{DFT}) and pore volume (V_{DFT}) were calculated using 2D-NLDFT approximations. Micropore specific surface area (S_{micro}) and micropore volume (V_{micro}) were also calculated using 2D-NLDFT.

X-ray diffraction method. The XRD patterns were collected with a Bruker D8 Advance diffractometer with Ni-filtered CuK_α radiation (0.6 mm wide parallel beam, two 2.5° Soller slits, and LynxEye line detector system). The scanning step of 0.01° for 2θ was applied from 10° to 90° and the total counting time per step was 166 s. The operating current of the X-ray tube was 40 mA, and the voltage was 40 kV. Full profile analysis was conducted for the catalyst materials, using Topas 6 software to calculate the lattice parameters and the size of Pt crystallites by modelling diffraction patterns. The measurements were carried out by Jaan Aruväli.

Thermogravimetric analysis. The content of Pt in the catalysts was determined by TGA, using NETZSCH STA 449 F3 Jupiter instrument. The content of Pt in the catalyst material was calculated based on the weight loss of the starting carbon support material and the catalyst material itself using Eq. 9. The assumption is that the carbon material with additives remains in its original form during the synthesis of the catalyst material, and only platinum is added to the starting material during synthesis. Meaning that the weight change would be only due to the oxidation of the carbon support.

$$\text{Pt content (wt\%)} = 100 - \frac{\text{Catalyst weight loss}}{\text{Carbon support weight loss}} \times 100 \quad (9)$$

Measurements were performed at a temperature range from 25 °C to 800 °C. The sample weight was approximately 10 mg, and the heating rate was 10 °C min^{-1}. The synthetic air flow rate was 50 cm^3 min^{-1}, and it consisted of 80% nitrogen (5.0, AS Linde Gas) and 20% oxygen (5.0, AS Linde Gas).

Scanning electron microscopy with energy dispersive X-ray spectroscopy. SEM-EDX examination was conducted with some of the studied materials using Zeiss ULTRA 55 SEM. The sample chamber was under high vacuum conditions. The InLens SEM images of the

materials were taken with different magnifications using signals of secondary electrons. The composition of the sample was determined using EDX analysis. The measurements were carried out by Olga Volobujeva (TalTech).

2.4. Rotating disc electrode measurements

Laboratory glassware washing. The laboratory glassware was placed in a concentrated sulphuric acid solution (SIGMA-ALDRICH, ACS Reagent, 95.0-98.0%), to which a small amount of hydrogen peroxide (EMSURE, ISO, 30%) was added. The mixture was previously heated to a temperature of 80 °C. The sulphuric acid solution was then allowed to cool for 30 min before rinsing the vessels with deionised water and MilliQ$^+$ water. The vessels were dried in a drying cabinet (BINDER FD 53 E2) at a temperature of 110 °C for 70 min.

Preparation of glassy carbon disc electrodes. Prior to RDE measurements, a glassy carbon electrode (PINE Instrument Company, S = 0.196 cm^2) was coated with a catalyst material. The electrode was polished to a mirror finish using 0.3 and 0.05 μm alumina oxide paste (Buehler, MicroPolish, Alumin) and cleaned ultrasonically in MilliQ$^+$ water. Catalyst suspension was prepared by mixing typically 6.3 mg of catalyst powder with a suitable amount of MilliQ$^+$ water and isopropyl alcohol. A few microliters of 1 M KOH solution was also added to the ink so that the pH of the ink was between 10 and 11. The ink mixture was sonicated for 15 min. After that, the suspension (9 μl) was applied to the glassy carbon electrode using a pipette. The Pt loading on the electrode was 18 μg_{Pt} cm^{-2}. The electrodes were dried on a hot plate (50 °C) in water and isopropyl alcohol vapour flow carried by N_2 gas. [38,39] Some examples of optical microscope images of the glassy carbon electrodes covered with different catalyst materials are shown in Appendix 1.

Rotating disc electrode measurement conditions. Measurements were conducted in a glass measuring cell. A glassy carbon electrode coated with catalyst material was used as the working electrode, a reversible hydrogen electrode (RHE) was used as the reference electrode, and a platinum wire was used as the auxiliary electrode. The working electrode was attached to a RDE device (PINE Instrument Company). The reference electrode was connected to the cell via a Luggin capillary. Measurements were carried out in a 0.1 M $HClO_4$ solution prepared from concentrated perchloric acid (Suprapur, Sigma-Aldrich, 70%). The RHE was prepared immediately before the measurements by electrolysing the acid solution and collecting the hydrogen using a chronoamperometric regime (−30 mA, 3 min). The measurements were conducted with at least three different glassy carbon electrodes until at least three overlapping results were measured. The acid solution was replaced with a new one after each electrode.

Before immersing the electrodes in the solution to be studied, a drop of MilliQ$^+$ water was applied to the electrode to help wet the catalyst layer. After immersing the electrode in the solution saturated with argon (6.0, As Linde Gas), the electrode was cycled in a range of potentials from 0.025 to 1.20 V vs. RHE at a scan rate of 500 mV s^{-1} [20]. Electrochemical impedance spectroscopy (EIS) measurements were then performed. The resistance determined from EIS was used to compensate for the ohmic drop in ECSA and ORR kinetics measurements. EIS was measured at a potential of 450 mV vs. RHE and frequencies ranging from 0.1 to 10000 Hz, with 51 points collected in a logarithmic scale and a potential amplitude of 0.01 V_{RMS}. The electrolyte resistance, *R*, was estimated by extrapolating the real part of the impedance, *Z'*, to an infinite frequency, *f* (*R* = *Z*' (*f*→∞)). To avoid overcompensation, CV was performed by varying the resistance until the potentiostat became unstable and the potential began to oscillate. The resistance used for compensation was between 18 and 24 Ω. CV measurements were carried out for ECSA determination in potential range from 0.02 V to 1.00 V vs. RHE and potential scan rates from 10 mV s^{-1} to 400 mV s^{-1}. The ORR kinetic measurements were performed at a scan rate of 20 mV s^{-1} and potential range from −0.01 V to 1.00 V. RDE measurements were made at an electrode rotation speed of 1 600 rpm. First, the electrolyte solution was saturated with argon and later with oxygen (5.0 As Linde Gas). To evaluate ORR kinetics, the current measured in an oxygen environment was subtracted from the current measured in an argon environment. Mass activity (MA) is the activity of a catalyst per unit of Pt mass, and specific activity (SA) is the activity of a catalyst per unit of the Pt ECSA. MA is calculated by dividing j_{kin} with m_{Pt} and SA is calculated by dividing j_{kin} with Pt ECSA [46].

A Metrohm Autolab potentiostat (Metrohm, Autolab B.V., PGSTAT302N, FRA32M, ADC10M, SCAN250) and NOVA 1.10.4 software were used for the measurements.

2.5. PEMFC single cell measurements

Preparation of the catalyst ink. A suspension was produced to prepare the MEA catalyst layer. The catalyst materials were suspended in MilliQ$^+$ water, Nafion solution (D521 NafionTM Solution, Ion Power, 5%), and isopropyl alcohol [47]. The components were taken in proportions to achieve the desired electrode surface concentration and ensure a uniform layer formation. The mixture was sonicated for 15 min (37 kHz, 100%, 0 °C), and then stirred (4 h, 14 600 rpm) using a HIGH-SHEAR T10 or T25 IKA Ultra mixer to obtain a homogeneous suspension. The suspension was mixed overnight using a magnetic stirrer at 750 rpm. Before

deposition, the suspension was sonicated for 15 min and stirred with a HIGH-SHEAR mixer for 1 h at 14 600 rpm.

Membrane electrode assembly preparation. For the PEMFC measurements, 5 cm^2 MEAs were prepared [47]. For the anode, a commercial catalyst 60% Pt on high surface area (HSA) Ketjenblack suspension was deposited onto a Nafion membrane (NAFION^{TM} Membrane HP, Ion Power) using an ultrasonic coating system Sono-Tek ExactaCoat. The loading of catalyst material on the anode was 0.1 mg cm^{-2}. For the cathode, the suspension of materials under investigation was applied to the membrane using an ultrasonic spray system or pipetted onto a GDL Freudenberg H23C3 Carbon Paper (FuelCellStore). Also, MEA hot-pressing was tested with CARVER. INC. manual heated hydraulic press (3 min, 125 °C, 265 kg of force) [48]. Hydrophobized carbon paper with a hydrophobic microporous layer (Freudenberg H23C3 Carbon Paper, FuelCellStore) was used as the GDLs for the anode and cathode. The loading of catalyst material for the cathode was 0.7 mg cm^{-2} or to get a Pt loading of 0.42 mg_{Pt} cm^{-2}. All the catalyst layers that were deposited onto a GDL were additionally coated with a Nafion layer (loading 0.068 mg_{Nafion} cm^{-2}) to achieve a better contact between the catalyst and the polymer electrolyte membrane [48].

Measurement conditions. The measurements were conducted in a 5 cm^2 PEMFC single cell. Autolab PGSTAT 302N with FRA32M and a BOOSTER20A were used using Nova software. A FUEL CELL TECHNOLOGIES INC. instrument was used to control the gas flow rate and humidity. The cell temperature was 62 °C, the temperature of the humidification vessels was 60 °C, and the gas line was 70 °C. The gas applied to the anode was H_2 (5.0, As Linde Gas), and the flow rate was 200 cm^3 min^{-1} at a pressure of 1.4 bar. Gas applied to the cathode side was air (As Linde Gas, Airapy: O_2 21.5%, N_2 78.5%), and the flow rate was 2 dm^3 min^{-1} at atmospheric pressure. After the cell reached measurement conditions, it was cycled between OCV and 0.4 V. After cycling, cell voltage in the current range from 0 A to the maximum current at 0.4 V was measured in 0.2 A steps (polarization and power curves were obtained).

For the ECSA evaluation, the single cell and humidification vessels were held at room temperature. H_2 was applied to the anode at atmospheric pressure, and the gas flow rate was 12 cm^3 min^{-1}. N_2 (5.0, As Linde Gas) was applied to the cathode at atmospheric pressure, and the gas flow rate was 200 cm^3 min^{-1}. The current vs. electrode potential data was measured in the potential range from 0.08 V to 1.00 V vs RHE at potential scan rates from 20 mV s^{-1} to 300 mV s^{-1}.

3. Results and discussion

3.1. Physical characterisation

3.1.1. Particle size analysis of the carbon support materials

The influence of milling on the particle size distribution of **PDC1** and **PDC2** is shown in Fig. 7. The mean diameter of particle sizes from the volume distribution is MV. The MVs of studied carbon materials are shown in Table 2.

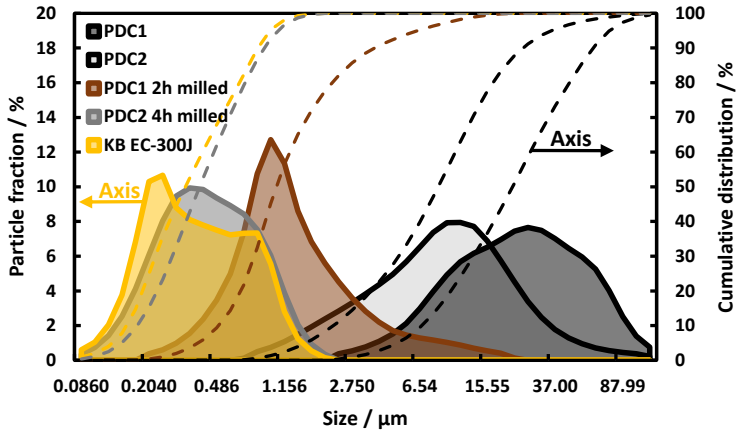

Figure 7. Particle size distribution of studied carbon support materials.

Table 2. Mean diameter of carbon particle sizes MV in the volume distribution.

Material	MV / µm
PDC1	28
PDC1 2h milled	1.8
PDC2	12
PDC2 1h milled	1.5
PDC2 2h milled	0.72
PDC2 3h milled	0.57
PDC2 4h milled	0.47
EG3	0.49
Ketjenblack EC-300J	0.42

The milling reduced the size of the PDC particles and increased the carbons' surface area. The carbon material's milling is necessary to prepare a stable suspension in the electrode preparation step. Smaller particle size helps to improve the homogeneity and stability of the suspension. The PDC was milled to decrease the particle size, after milling the particle size was small enough, and the suspensions made from the synthesised materials were stable for at least one hour.

Fig. 8a illustrates the gradual particle size decrease of the **PDC2** carbon particle size. During the milling of **PDC2**, the MV values were registred hourly (Table 2), although the decrease was significantly smaller and almost nonexistent after 3 h of milling. After 4 h of milling, the MV value of the PDC2 was similar to the MV value of the commercial carbon Ketjenblack EC-300J (the size distributions were also almost identical, shown on Fig 7).

To show that Pt deposition onto the carbon support does not affect the particle size distribution, particle size measurements with materials **PDC2**(4h milled) and **EG3** were used as an example. In Fig. 8b, the size distribution of **PDC2**(4h milled) and **EG3** have the same shape, and the difference between the MV values is almost non-existent. Other catalysts and support materials behave in the same manner.

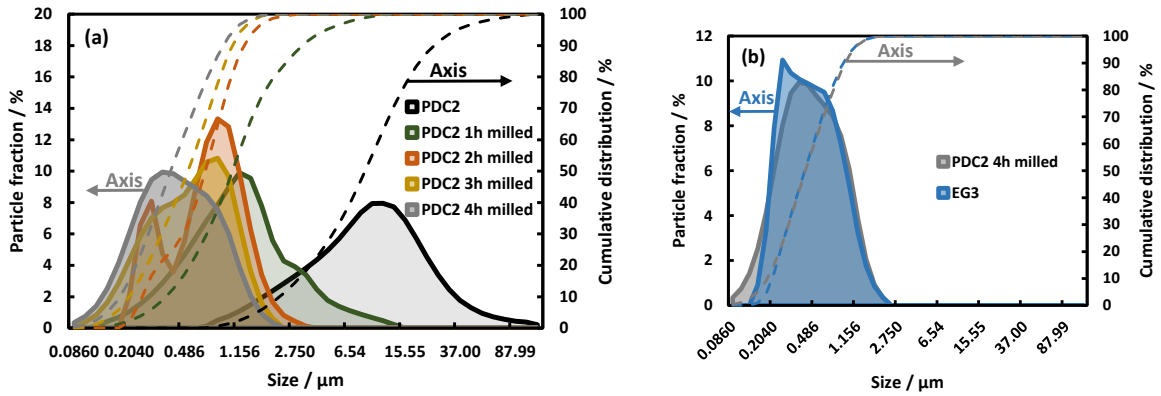

Figure 8. Effect of milling on the **PDC2** materials particle size distribution **(a)**. Particle size distribution of the **PDC2**(4h milled) and **EG3** materials **(b)**.

3.1.2. Specific surface area and porosity measurements

Based on N_2 sorption measurements, the pore size distribution and specific surface area of the materials were evaluated. The results of N_2 sorption measurements are shown in Fig. 9 and Table 3. The pore size distributions calculated by the 2D-NLDFT mainly describe micro- and mesopores, as pores larger than 30 nm are not taken into account. Therefore the amount of micropores may be somewhat overestimated [44,45].

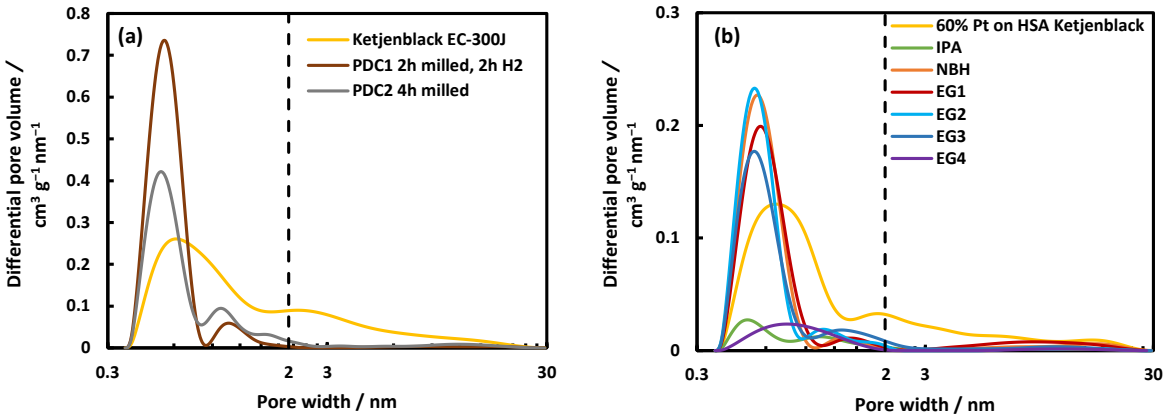

Figure 9. The pore size distribution of the investigated carbon supports **(a)** and catalysts **(b)**.

All synthesised materials are micro-mesoporous (mesopores have a diameter of 2–50 nm, micropores ≤ 2 nm [49]). The commercial materials 60% Pt on HSA Ketjenblack and Ketjenblack EC-300J are more mesoporous than the synthesised materials. Precipitation of Pt nanoparticles onto the PDC materials decreased the proportion of micropores, which can be explained by the deposition of Pt nanoparticles into the micropores. For commercial materials, the catalyst's specific surface area and pore volume constitute approximately 40% of the carbon support values. This indicates that the porous structure of the carbon was not altered during the Pt deposition process. However, this was not the case for the syntheses performed in this work,

particularly with significant changes observed in the **IPA** and **EG4** materials. The specific surface area of the investigated catalyst materials prepared using various synthesis methods decreased in order: **NBH** > **EG1** ≥ **EG2** > **EG3** > **EG4** ≥ **IPA**. The quotient V_{micro}/V_{DFT} shows the proportion of micropores in the material, and the results show that the microporosity of the synthesised materials is higher than the commercial materials. The proportion of micropores does not change for the commercial material after Pt deposition. This shows that the Pt was deposited uniformly into the pores of the carbon support. In the case of materials using **PDC1**(2h milled, 2h H_2), the proportion of micropores significantly drops after the Pt deposition, and this can be explained by the uneven Pt nanoparticle deposition or some other factor that clogged the micropores during the synthesis. For catalysts synthesised with **PDC2**(4h milled) as a support material, the proportion of micropores drops only for material **EG4** due to overall porosity collapse.

Table 3. The results of N_2 sorption measurements.

Material	S_{DFT} / $m^2\ g^{-1}$	S_{micro} / $m^2\ g^{-1}$	V_{DFT} / $cm^3\ g^{-1}$	V_{micro} / $cm^3\ g^{-1}$	V_{micro}/V_{DFT}
Ketjenblack EC-300J	730	527	0.78	0.23	30%
PDC1(2h milled, 2h H_2)	658	646	0.25	0.19	76%
PDC2(4h milled)	481	453	0.27	0.15	56%
IPA	45	40	0.037	0.016	43%
NBH	242	226	0.16	0.069	43%
EG1	233	211	0.18	0.067	39%
EG2	227	222	0.097	0.068	71%
EG3	203	191	0.11	0.064	57%
EG4	47	44	0.036	0.019	52%
60% Pt on HSA Ketjenblack	308	239	0.33	0.10	31%

S_{DFT} – 2D-NLDFT surface area S_{mikro} – 2D-NLDFT micropore surface area
V_{DFT} – 2D-NLDFT pore volume V_{mikro} – 2D-NLDFT micropore volume

3.1.3. Results of X-ray diffraction measurements

The collected XRD data is presented in Fig. 10. In Fig. 10a, all the carbon support materials exhibit distinguishable characteristic XRD reflexes to amorphous carbon, corresponding to planes C(002) and C(100/101) [17]. In the case of **PDC1**(2h milled, 2h H_2) material, reflexes of quartz, silicates, and iron compounds are visible because the source material (peat) comes from nature, and some impurities remain in the carbon material. **PDC1**(2h milled, 2h H_2) also had ZrO_2 and titanate reflexes. These compounds were most likely introduced into the carbon material during milling. Material **PDC2**(4h milled) has fewer natural additives (SiO_2). XRD results show that the additives in PDC2 material are more difficult to detect, this does not mean additives do not exist. It could be that during the 4 h milling step with small 1 mm balls, the additives got a more amorphous nature (or the particles were milled so small) that they became

undetectable with the XRD method. In the commercial carbon black Ketjenblack EC-300J, no additives were found. Compared to other studied carbon materials, the commercial carbon had somewhat narrower reflexes, indicating that the commercial carbon has a slightly more ordered structure.

In Fig. 10b, all the catalyst materials have characteristic Pt reflexes that are very clearly visible, corresponding to the Pt(111), Pt(200), Pt(220), Pt(311), and Pt(222) planes [33]. Commercial carbon has broader and less intensive reflexes because Pt has a less ordered structure and a smaller crystallite size. The width of the reflexes of the studied catalyst materials increases in the same order as the Pt crystallite size decreases shown in Table 4. The Pt crystallite sizes increase in order: **60% Pt on HSA Ketjenblack** < **EG1** < **EG4** < **EG3** = **EG2** < **NBH** < **IPA**.

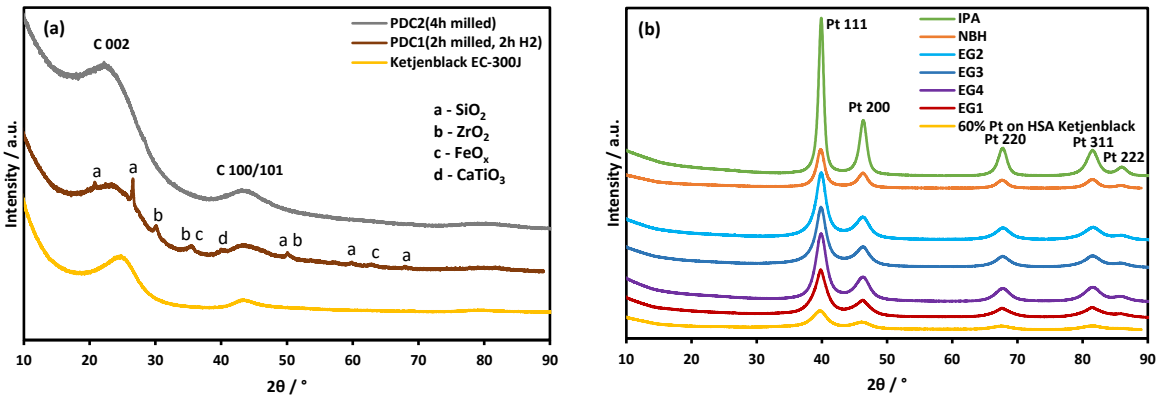

Figure 10. X-ray diffraction patterns of the studied carbon supports **(a)** and catalysts **(b)**.

The lattice parameter, Pt crystallite size and Pt content of the studied catalyst materials are shown in Table 4. The lattice parameter for the studied materials varies between 3.91 and 3.92 Å. This is less than a = 3.9236 ± 0.0006 Å, reported in the literature [50]. It has been shown in the literature that when the size of the Pt crystallite is small, the Pt lattice parameter is also smaller than usual [51]. The result obtained can therefore be considered reasonable.

Table 4. Pt crystallite size, lattice parameter, and Pt content of the studied catalyst materials.

Material	Pt crystallite size d_{Pt} / nm	Lattice parameter a / Å	Pt content / wt%
IPA	6.0	3.916 ± 0.001	58.6
NBH	4.0	3.915 ± 0.001	60.4
EG1	2.4	3.920 ± 0.011	59.1
EG2	3.0	3.916 ± 0.011	59.3
EG3	3.0	3.916 ± 0.016	58.4
EG4	2.9	3.917 ± 0.001	56.3
60% Pt on HSA Ketjenblack	1.9	3.906 ± 0.007	60.0

3.1.4. Thermal stability and Pt content of the materials

TGA was used to assess the thermal stability of the materials. Also, to determine the quantity of additives and the content of Pt in the synthesised materials. TGA results are shown in Fig. 11. The significant weight loss between 300 °C and 700 °C corresponds to the oxidation of carbon. The weight change at around 100°C likely corresponds to water evaporation. The temperature at which the weight of the catalyst materials reached 90 wt% could be used to describe the thermal stability of the synthesised materials. The carbon support materials are thermally more stable than the catalyst materials because catalysts contain platinum, making them more reactive. Only catalyst material to be more stable than its support material is **IPA**. Commercial carbon is significantly more thermally stable than the synthesised carbon supports due to lack of additives in the material, and because of more graphitised structure (Fig. 10a). The temperature at which the synthesised catalyst materials reached 90 wt% of their initial value increases in order: **EG3** = **EG2** < **EG1** < **EG4** < **NBH** < **IPA**. This correlates somewhat to the Pt crystallite size which increases in a similar fashion shown in Table 4 (except materials **EG3** and **EG2**). This indicates that the catalyst materials with larger Pt crystallite size react with oxygen at higher temperatures, making them thermally more stable, although less electrochemically active (Chap. 3.2.1.). Fig 10a shows that PDC materials are not entirely composed of carbon. The carbon oxidises fully before the synthesised support materials weight % reaches zero, the residue left are additives in the PDC. It seems that **PDC2**(4h milled) has more additives, this may be due to a longer milling time. The calculated wt% of Pt in the catalyst materials is shown in Table 4. The Pt mass percentage calculated from TGA results confirm that catalyst materials with about 60 wt% Pt content were synthesised.

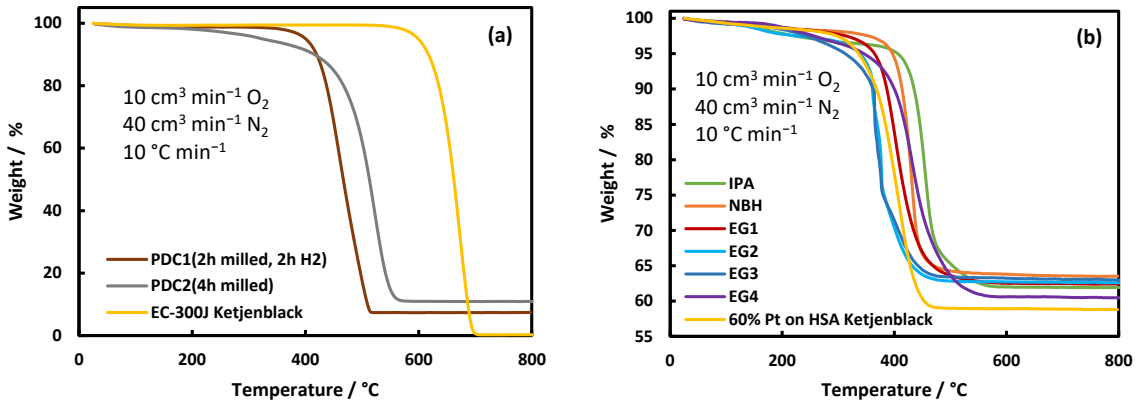

Figure 11. Thermogravimetric analysis of the carbon supports **(a)** and the catalysts **(b)**.

3.1.5. Morphology and elemental composition of IPA, NBH and EG1 materials

SEM images of materials **IPA**, **NBH**, and **EG1** are shown in Fig. 12. The effect of milling is seen in Fig. 12a. The dimensions of the carbon support particles measured directly from SEM are primarily around 1 μm (Fig. 7). A (macro)porous structure can be observed. Pt particles (white) are deposited inside the opened pores and onto the carbon. SEM image of the **EG1** material, synthesised using ethylene glycol as a reduction agent, is shown in Fig. 12a. For the **EG1** material, the Pt nanoparticles are uniformly dispersed onto/into the carbon particles forming a "web-like" structure. As a comparison, Fig. 12c shows SEM images of **NBH** material. The Pt particles on the **NBH** material are more agglomerated and not so well dispersed. In Fig. 12d, large round Pt nanoclusters can be seen. The **IPA** material is not evenly covered by Pt nanoparticles at all, also there are large, agglomerated Pt nanoclusters visible. This is in accord with XRD data (Table 4) that shows Pt crystallite sizes of the materials increasing in order: **EG1** < **NBH** < **IPA**. The dispersion of Pt nanoparticles is better for the **EG1** material. The SEM images show that using ethylene glycol as a reducing agent for the Pt catalyst synthesis gives a better dispersion of Pt nanoparticles and a smaller Pt particle size.

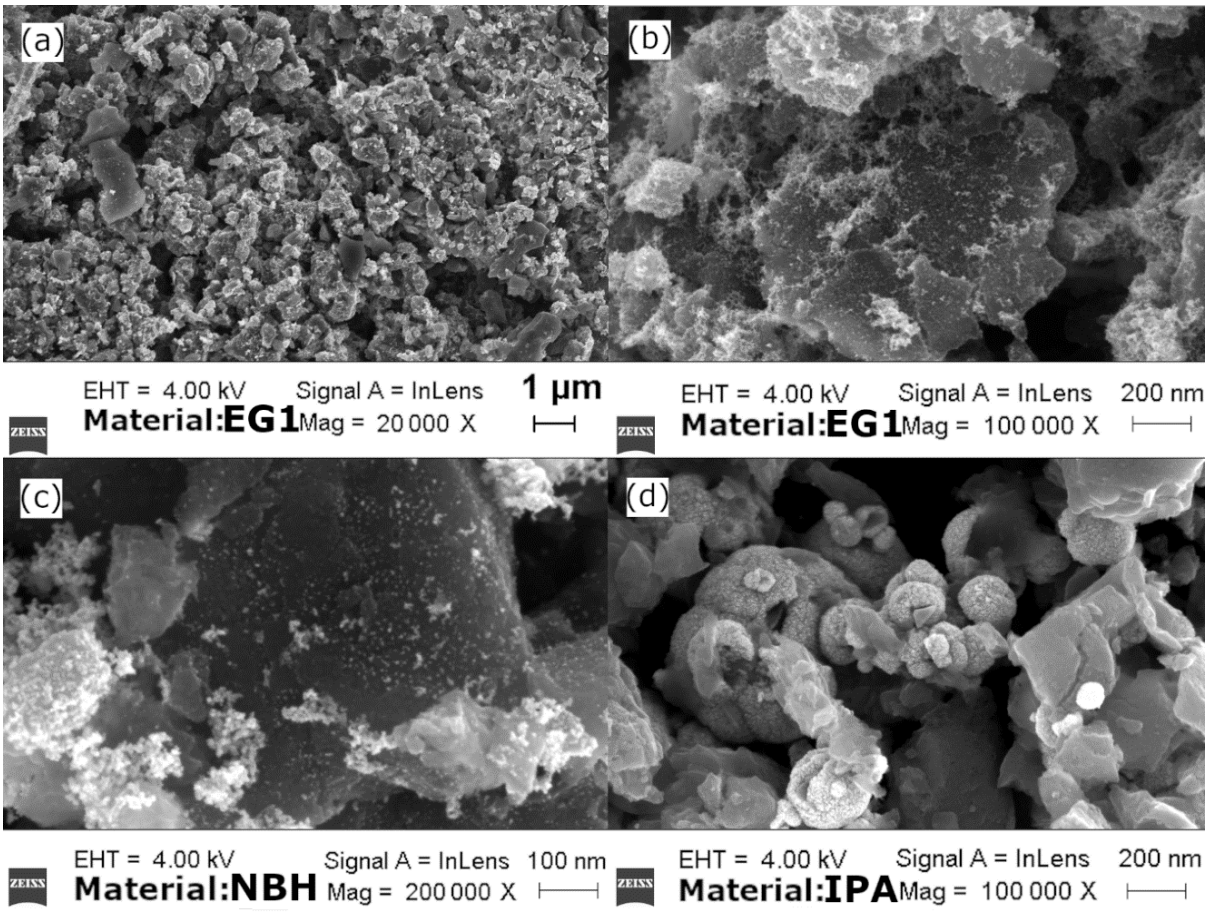

Figure 12. Scanning electron microscopy images of materials **IPA**, **NBH**, and **EG1**.

EDX data was used to confirm the chemical composition of the synthesised catalyst materials. The EDX analysis showed that all synthesised catalyst materials contain carbon, oxygen, and platinum. The EDX data did not reveal the existence of impurities in the materials, except for small amounts of silicon and chlorine.

3.2. Electrochemical measurements

3.2.1. Results of the rotating disc electrode measurements

All the studied catalyst materials were electrochemically characterised in a three-electrode system in 0.1 M $HClO_4$ solution using the RDE method to measure the ORR activity. RDE experiments allow for a simplified and focused assessment of the catalyst's behaviour, separate from all the complexities of a PEMFC system. The results of the three-electrode system measurements are summarised in Table 5.

Table 5. Results of the rotating disc electrode measurements.

Material	ECSA / $m_{Pt}^2\ g^{-1}_{Pt}$	$-j_d$ / A m^{-2}	$-j_{kin}$ / A m^{-2}	MA / A g^{-1}_{Pt}	SA / A m^{-2}_{Pt}	Tafel slope / mV
			@ 0.9 V vs. RHE			
60% Pt on HSA Ketjenblack EC-300J	58.1	59.7	51.2	284	4.9	55
IPA	8.8	50.8	10.1	56.0	6.3	60
NBH	5.2	52.5	5.7	31.5	6.1	56
EG1	20.6	58.1	25.4	141	6.9	57
EG2	25.6	59.6	24.7	137	5.4	56
EG3	26.0	56.9	27.8	159	6.1	59
EG4	33.4	59.5	50.1	278	8.3	55

ECSA – electrochemically active surface area, j_d – diffusion limited current density at 1 600 rpm, j_{kin} – kinetic current density, MA – mass activity, SA – specific activity,
Tafel slope region: 0.90…1.00 V vs. RHE.

The dependences of calculated gravimetric capacitance on the electrode potential for the synthesised materials in a three-electrode system are shown in Fig. 13a. The ECSA values were calculated using the CV data according to the ECSA calculation method provided in Chap. 1.7. *C*,*E*-dependences shown in Fig. 13a were calculated from the measured *j*, *E*-dependences. In a three-electrode system, the ECSA values of the synthesised catalysts decrease in order: **EG4** > **EG3** ≥ **EG2** > **EG1** > **IPA** > **NBH**. The shapes of the curves are characteristic of the Pt catalyst. Different characteristics, like hydrogen and oxygen ads/des areas, are clearly distinguishable, the curves show sharp peaks in the hydrogen ads/des area characteristic of Pt catalysts. The sharp hydrogen peaks are better developed for materials with higher ECSA values. The potential of hydrogen ads/des peaks is the same for all the studied materials, and the peaks potential values for the anode and cathode are approximately the same. The smaller the

difference in their potentials, the purer the electrolyte solution can be considered. Also, *C*,*E*-curves do not show additional peaks (in the EDL region), indicating that the electrolyte solution and cell were thoroughly cleaned. In the hydrogen ads/des region, the peak heights decrease in the following order: **EG4** > **EG2** > **EG3** > **EG1** > **IPA** > **NBH**. This is in good agreement with the ECSA values. Furthermore, the ECSA values in this order correspond somewhat to the increase of Pt crystallite size (Table 4), except for the material **EG1**. This shows that Pt crystallite size strongly affects the material's ECSA value. The smaller the Pt crystallite size, the higher the ECSA value. The commercial material has a significantly smaller Pt crystallite size, therefore a much larger ECSA value than the synthesised materials.

Using the RDE method, the dependence of the measured ORR current density, j_c, on the electrode potential was found, Fig. 14a. Distinct charge transfer, mixed kinetics, and mass transfer regions are clearly distinguishable for all materials. The theoretical diffusion-limited current density values were almost achieved for the EG1, EG2, EG3, EG4, and the commercial catalyst (n = 4). Materials IPA and NBH did not achieve this because the activity of these materials is too low.

Table 5 presents the studied materials' j_{kin}, MA, and SA at a potential of 0.9 V vs. RHE. The MA and j_{kin} values show that the activity of the synthesised materials decreases in order: **EG4** > **EG3** > **EG1** > **EG2** > **IPA** > **NBH**. Comparing the activity values and ECSA values in Table 5 with Pt crystallite sizes in Table 4, a obvious correlation appears: the smaller the Pt crystallite size, the higher the ECSA values, the more active the material. Therefore, ECSA (as well as Pt crystallite size) strongly affects the activity of a Pt catalyst. The correlation between the ECSA and MA of the studied catalysts in a three-electrode system is shown in Fig. 13b. Material **EG4** deviates from the trendline and shows a very high MA compared to the ECSA of the material. This shows, that **EG4** is a very active material, and with further development could potentially reach the MA values of the commercial material or even higher.

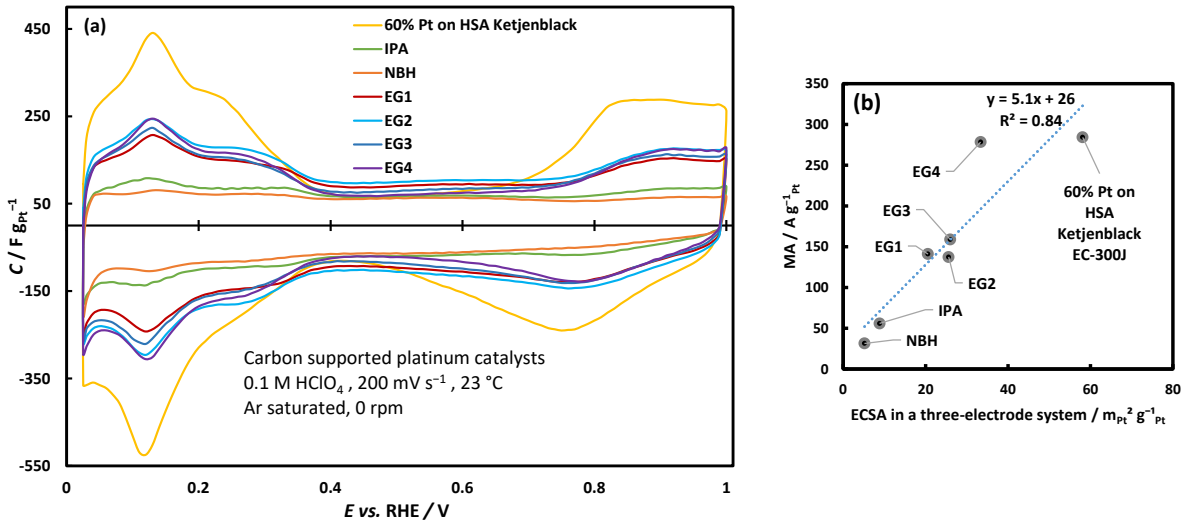

Figure 13. Dependence of the calculated gravimetric capacitance on the electrode potential **(a)** and the correlation between the mass activity and the electrochemically active surface area **(b)** for the studied catalysts in a three-electrode system in 0.1 M $HClO_4$ solution.

Tafel dependencies, shown in Fig. 14b, were used to analyse the charge transfer kinetics. From the RDE data, the kinetic currents values per mass of Pt (A g_{Pt}^{-1}) were calculated using the K-L equation (Eq. 4). In the region of low current densities, the Tafel dependencies are linear, and their slope values are provided in Table 5. The Tafel slopes range from 55 mV to 60 mV and do not significantly depend on the catalyst in the region of low current densities $|j_c|$ (where the potential range is 0.90…1.00 V vs. RHE). This is in accordance with the literature [52]. In the region of higher current densities (where the potential is lower than 0.80 V vs. RHE), the Tafel slope becomes steeper, which could be attributed to a change in the charge transfer mechanism or deviations resulting from a non-ideal catalyst layer and thus, a simple K-L model does not apply [53].

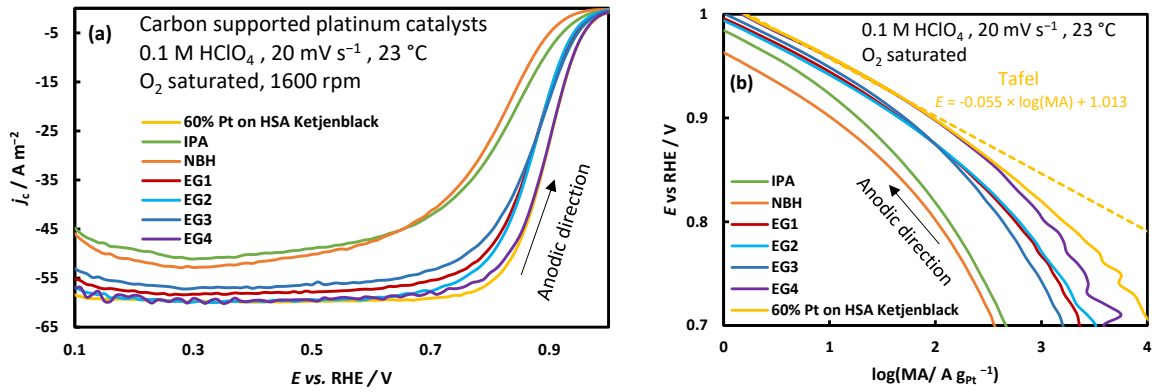

Figure 14. Oxygen reduction reaction rotating disc electrode measurement data **(a)** and Tafel dependences **(b)** of the synthesised and commercial Pt catalyst materials in a three-electrode system in 0.1 M $HClO_4$ solution.

3.2.2. Optimisation of the PEMFC catalyst layer deposition method

When assembling a PEMFC, the methods of applying the catalyst material are very important. Typically, the catalyst material is applied directly to the membrane. This ensures a low contact resistance between the membrane and the catalyst layer. The application of catalyst materials directly onto the GDL is also used [54], which creates a good connection between the catalyst and the GDL. A poor connection can cause water accumulation between the GDL and the catalyst material, hindering the reactant transport. To reduce the resistance between the catalyst layer applied onto the GDL and the membrane, a thin ionomer top layer is applied over the catalyst layer [48]. Assembling the MEA by hot pressing has also been tried to reduce resistance. Hot pressing is necessary to achieve good contact between the membrane, catalyst layer, and GDL [48]. The method of applying the catalyst material suspension onto the GDL is also important. One approach is to pipette the suspension onto the surface of the GDL and wait for it to dry [55]. As a faster coating method, an automated ultrasonic spraying system can be used, resulting in a more uniform layer of catalyst material than pipetting [47].

The above-mentioned catalyst material application methods were used to find out the optimal way to prepare a MEA with the studied catalyst materials. As an example, Fig. 15 shows the PEMFC single cell measurements of five different coating methods tested with the material **EG1**.

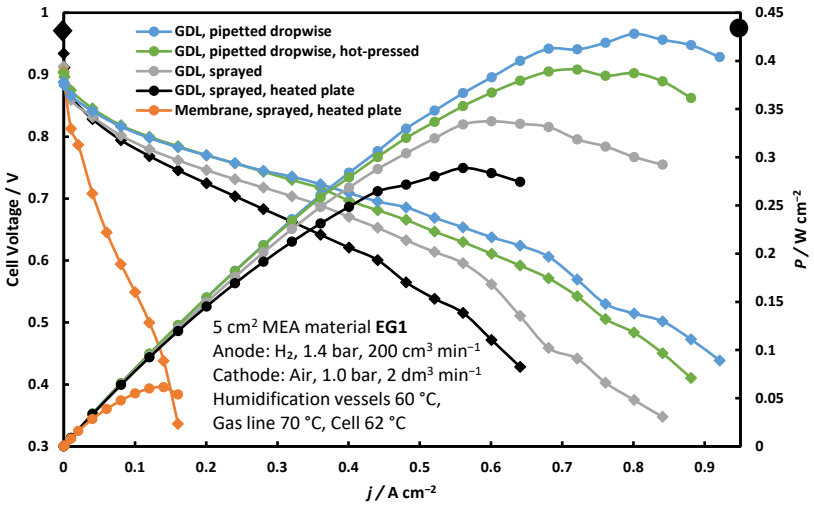

Figure 15. Proton-exchange membrane fuel cell single cell measurement results of **EG1** material with five different catalyst coating techniques. Dependence of cell voltage (squares) and power density (circles) on current density applied.

The differently prepared MEAs with catalyst **EG1** were compared based on the maximum power density in a PEMFC single cell shown in Fig. 15. The order in which the maximum power density increased correlated with the order of maximum current density in the kinetic area of the polarization curve (at 0.7 V). The ECSA values were higher for better performing

MEAs. There was no significant change observed in the OCV and electrolyte resistance. The OCV values remained consistent within the 882 mV to 927 mV range, while the resistance was measured between 9.6 and 13.9 mΩ at −450 mV compared to the OCV.

The MEA with the lowest performance (P_{max} = 0.061 W cm^{-2}) was prepared using the method where the cathode was directly sprayed onto the Nafion membrane using an ultrasonic spray system on a heated plate. The spray system covered the membrane with the suspension very evenly, and because of the heated plate the material probably dried tightly together. This may have caused the material to form a very tight layer, which hindered the transport of reagents and water. This method is the best way to apply the commercial catalyst, but it does not seem to work with the PDC-based catalysts due to differences in structural characteristics (particle size distribution and surface functionalisation of the carbon support, the porosity of the catalyst, etc.). It was found that the MEAs with the best performance were those where the synthesised cathode catalyst material layer was applied onto the GDL. When the GDL was coated with the ultrasonic spray system on a heated plate, the material layer probably remained tight due to the fast evaporation of solvents. However, when coated at room temperature, the material showed a higher maximum power density because the solvents evaporated more slowly (similar to the pipetting method) and formed probably a more porous layer for reactant and water transport. The MEA with the highest maximum power density (P_{max} = 0.42 W cm^{-2}) was coated by pipetting the suspension onto the GDL dropwise. When the catalyst material layer of the suspension was slowly dried at room temperature, a porous layer was formed. Hot pressing was also tried to achieve better contact between the material applied to the GDL and the Nafion membrane. As a result, the maximum power density decreased slightly, but kinetic activity remained the same. During hot-pressing, the catalyst material was probably pressed too tightly together, the transport (macro-meso)porosity decreased, and transport of reactant and water were hindered. The different coating techniques were tested with all the synthesised materials. Pipetting the suspension onto the GDL dropwise was the method, that achieved the highest performing MEAs for all materials except commercial.

3.2.3. Addition of different dimensional carbon materials to a synthesised catalyst

To achieve even higher maximum power densities in a PEMFC single cell, adding commercial carbons such as CNT or carbon black Ketjenblack EC-300J to a synthesised catalyst was tested. Adding different dimensional carbon materials to the PEMFC catalyst layer has been shown to be an effective way to improve the fuel cell performance [40–42]. The PEMFC single cell measurement results, with the highest performing catalyst layer deposition method (pipetting

the suspension onto the GDL dropwise), with different additives: **EG3 + NT** and **EG3 + KB**, compared to the original catalyst **EG3** are shown in Fig. 16. During the measurements, there was no significant change observed in the OCV and resistance values. The OCV values remained within the range of 914 mV to 959 mV, and the resistance measured for both MEAs was 11.9 mΩ at −450 mV vs OCV shown in Table 6. High OCV and low resistance values show that there is a good contact between the catalyst and ionomer.

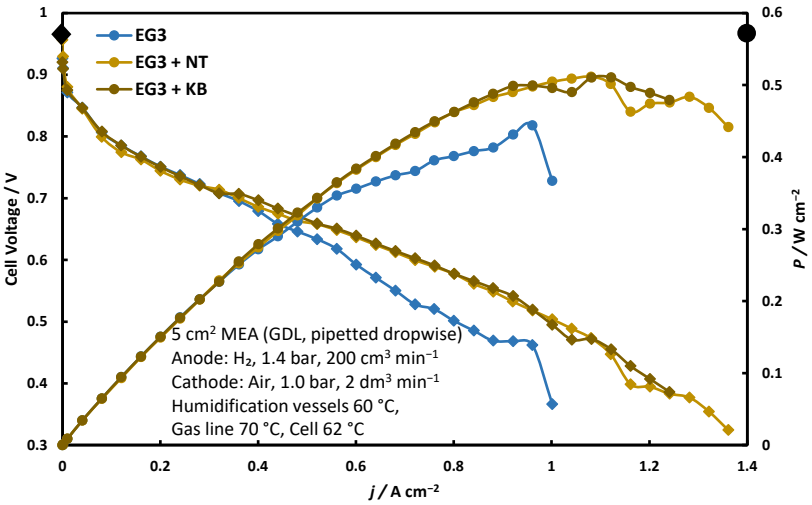

Figure 16. Proton-exchange membrane fuel cell single cell measurement results of **EG3**, **EG3 + NT**, and **EG3 + KB**. Dependence of cell voltage (squares) and power density (circles) on current density applied.

The addition of CNT (**EG3 + NT**) or carbon black (**EG3 + KB**) to **EG3** had a similar effect. Both additives have a mesoporous structure and a large specific surface area, providing a smooth mass transport of reagent gas (air) and water and high current values in the mass transfer region of the polarization curve. Probably the additives avoid tight packing of the catalyst layer, and therefore the catalyst achieves better performance in the mass transport area (higher maximum power density). Due to the additives' structural properties, the maximum power density of a MEA with **EG3** catalyst on the cathode (P_{max} = 0.45 W cm^{-2}) was surpassed noticeably by a MEA prepared with **EG3 + KB** (P_{max} = 0.53 W cm^{-2}) having the highest maximum power density of all the synthesised materials. **EG3 +NT** (ECSA = 25 m_{Pt}^2 g_{Pt}^{-1}) and **EG3 + KB** (ECSA = 21 m_{Pt}^2 g_{Pt}^{-1}) also exhibited higher ECSA values than the original **EG3** catalyst (ECSA = 19 m_{Pt}^2 g_{Pt}^{-1}). By adding CNT or carbon black to a synthesised catalyst, the ECSA and P_{max} values increased.

3.2.4. Results of the PEMFC single cell measurements

Table 6 presents a comparison of all PEMFC single cell measurements of the synthesised materials and commercial using the highest-performing MEA preparation method for each

catalyst. The power maximums of the materials decrease in order: **60% Pt on HSA Ketjenblack** > **EG3 + KB** > **EG3 + NT** > **EG2** > **EG3** > **EG1** > **EG4** > **NBH** > **IPA**.

Table 6. Results of the proton-exchange membrane fuel cell single cell measurements.

Material	ECSA / $m_{Pt}^2\ g_{Pt}^{-1}$	ECSA St. Dev.	OCV / mV	j / A cm^{-2}			P_{max} / W cm^{-2}	R / mΩ
				750 mV	700 mV	670 mV		−450 mV vs. OCV
IPA	9.5	0.5	633	-	-	-	0.03	-
NBH	5.8	0.3	954	0.12	0.19	0.23	0.24	12.3
EG1	22	1.1	882	0.26	0.43	0.52	0.42	9.6
EG2	18	1.0	915	0.20	0.34	0.43	0.47	11.6
EG3	19	0.4	927	0.21	0.35	0.42	0.45	11.8
EG3 + NT	25	0.6	959	0.19	0.36	0.48	0.51	11.9
EG3 + KB	21	0.4	914	0.20	0.39	0.52	0.53	11.9
EG4	23	1.3	970	0.22	0.35	0.44	0.40	12.0
60% Pt on HSA Ketjenblack	56	0.9	977	0.47	0.70	0.80	0.59	9.6

Anode: H_2, 1.4 bar, 200 cm^3 min^{-1}. Anode catalyst loading: 0.04 mg_{Pt} cm^{-2}.
Cathode: Air, 1.0 bar, 2 dm^3 min^{-1}. Cathode catalyst loading: 0.42 mg_{Pt} cm^{-2}.
Humidification vessels 60 °C, Gas lines 70 °C, Cell 62 °C, 5 cm^2 MEA.
ECSA – the electrochemically active surface area of platinum, OCV – open circuit voltage,
j – current density, P_{max} – maximum power density, R – resistance.

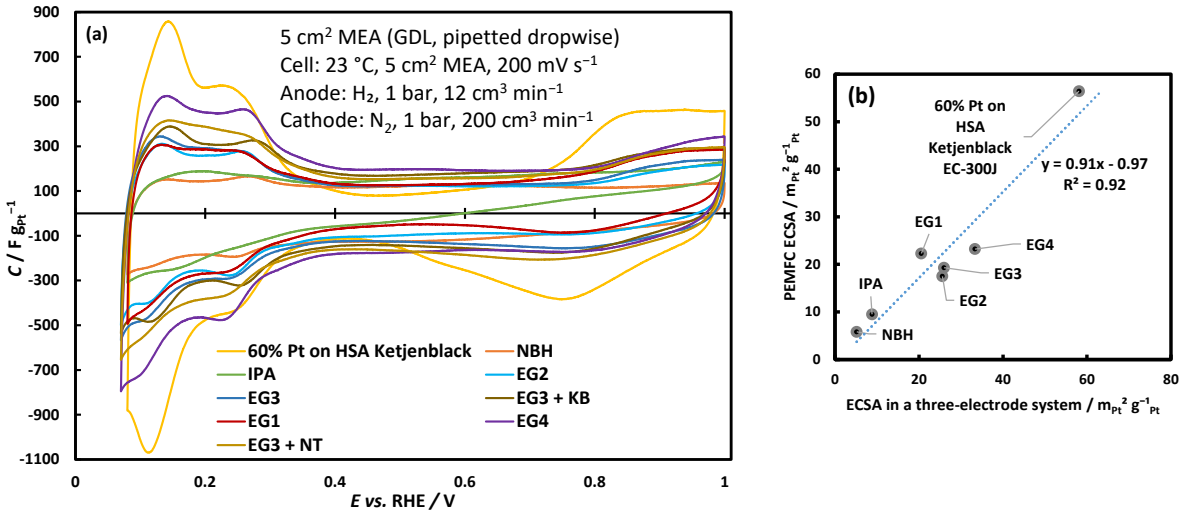

Figure 17. Dependence of the calculated gravimetric capacitance on the electrode potential in a proton-exchange membrane fuel cell single cell **(a)** and the correlation between the electrochemical activities of the materials in a three-electrode system and in a proton-exchange membrane fuel cell single cell **(b)** of the studied catalysts.

The dependence of calculated gravimetric capacitance on potential, for the synthesised materials in PEMFC single cell, are shown in Fig. 17a. The ECSA values were calculated using the method provided in Chap. 1.7. The calculated ECSA values are shown in Table 6. The shapes of the curves are similar to the usual shape of Pt catalyst *C*,*E*-curves in inert atmosphere. Different characteristics are clearly distinguishable, like hydrogen and oxygen ads/des areas (except maybe oxygen ads/des areas for material **IPA**). All catalyst materials have a relatively

large gravimetric capacitance in the EDL region. The large capacitance in the EDL and hydrogen ads/des area indicates that the Nafion chains are probably in good contact with the catalyst support particles. The order in which the ECSA values of the catalysts decrease in a PEMFC is: **EG4** > **EG1** > **EG3** > **EG2** > **IPA** > **NBH**. This order correlates with the ECSA values measured in in a three-electrode system, the correlation is shown in Fig. 17b.

Fig. 18a presents a comparison of maximum power density, current density at 700 mV, and ECSA for each material when the coating method was optimised (dropping the suspension drop-wise onto the GDL using a pipette was used in case of synthesised catalysts). The lowest activity was observed for the **IPA** and **NBH** material, while materials **EG1**, **EG2**, **EG3**, and **EG4** exhibited higher activity, accompanied by the higher ECSA values. The current density at 700 mV of the studied catalyst materials (except **EG3 + NT** and **EG3 + KB**) decreases in the same order as Pt crystallite size increases: **EG1** > **EG4** > **EG3** > **EG2** > **NBH** (> **IPA)**. Kinetic (activation) losses on the polarisation curve are smaller when the Pt crystallite size is smaller. The ECSA values of the studied catalysts also somewhat follow the same order, with a slight difference of **EG1** and **EG4** having switched places and adding of the **IPA** results. The order in which the ECSA values of the studied catalysts decrease is **EG4** > **EG1** > **EG3** > **EG2** > **IPA** > **NBH**. Smaller Pt crystallite size leads to higher ECSA values and, therefore, higher current densities in the kinetic region of the polarization curve, this correlation is shown in Fig. 18b. ECSA value is one of the factors that strongly affect the PEMFCs activity [56]. Better activity in the kinetic area of the polarization curve is important because minimizing activation losses is crucial to PEMFC performance.

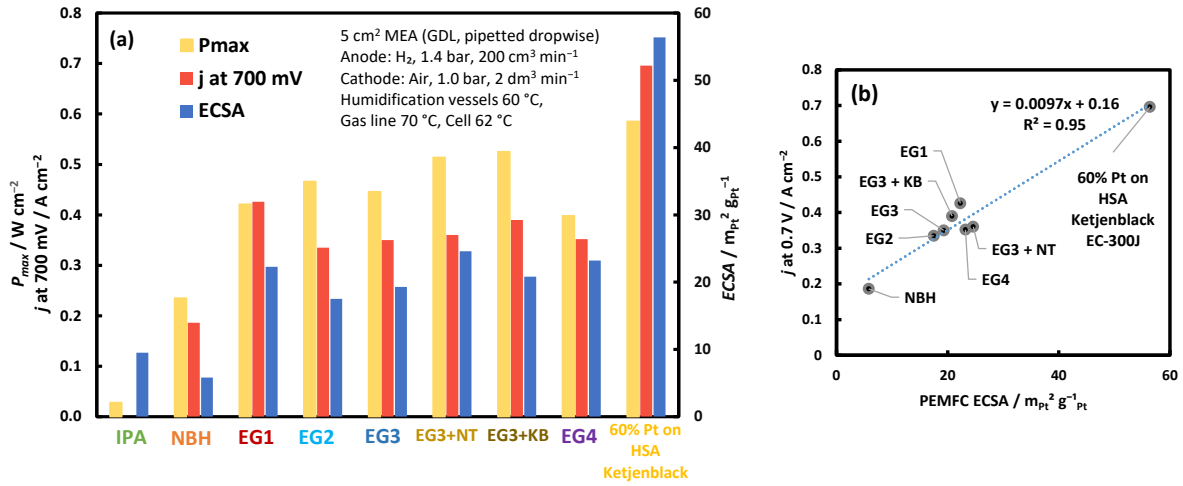

Figure 18. Comparison of maximum power density, current density at 700 mV, and electrochemically active surface area **(a)** and the correlation between the electrochemically active surface area and the current density at 0.7 V **(b)** of the studied catalysts in proton-exchange membrane fuel cell.

A comparison of the polarization curves of the best performing synthesised materials and the commercial catalyst 60% Pt on HSA Ketjenblack are shown on Fig. 19. The activity of all

synthesised materials is lower than that of the commercial material. Further research and development i.e. Pt nanoparticles depostion, formation of catalyst layer etc. work is required to reach the level of the commercial material.

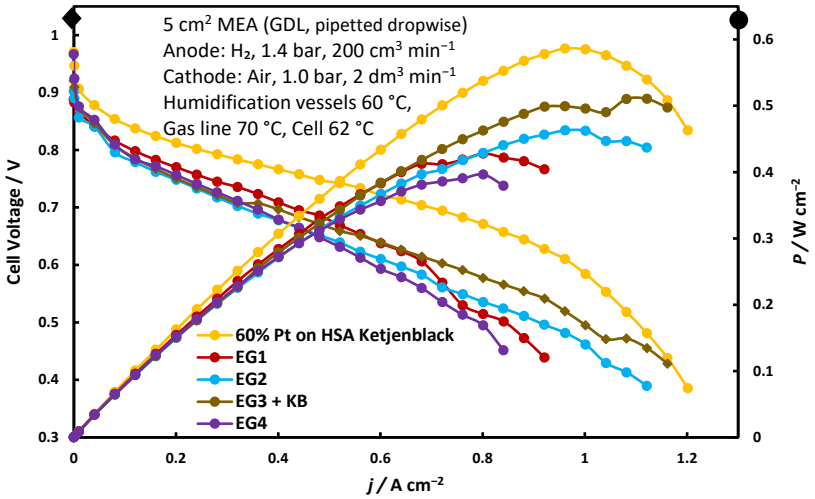

Figure 19. Proton-exchange membrane fuel cell single cell measurement results of best performing synthesised materials (optimised catalyst deposition method) compared to commercial 60% Pt on HSA Ketjenblack. Dependence of cell voltage (squares) and power density (circles) on current density applied.

The highest current density of 0.43 A cm^{-2} at 700 mV by a synthesised material with no additives was achieved by material **EG1**. The high activity in the kinetic area of the polarization curve is most likely because of the **EG1** materials high ECSA value (and a small Pt crystallyte size of 2.4 nm, the smallest of all synthesised materials). The highest maximum power density of 0.47 W cm^{-2} by a synthesised material with no additives was achieved with the material **EG2**. And the highest maximum power density of 0.53 W cm^{-2} of all the synthesised materials was achieved by **EG3 + KB**. The high current values in the mass transport region of the polarization curve are explained by better water management and reactant gases in the MEA having better access to the catalyst. Material **EG4**, although very active in the RDE experiments (MA of 278 A g^{-1}_{Pt} is comparable with the MA of the commercial catalysts 284 A g^{-1}_{Pt}), did not have a high performance in the PEMFC single cell, as the maximum power density and current density at 0.7 V were not the highest of the measured materials. The causing factors, why **EG4** did not have a high performance in the PEMFC, could be the collapse of porosity after the Pt deposition, or that the extensive ball milling of the support material particles increased the mass transfer losses. All the measured materials exhibited low resistance values, remaining consistent within the range of 9.6 to 12.3 mΩ at −450 mV.

Summary

This study focused on the development of Pt catalysts deposited onto a carbon support synthesised from Estonian peat for PEMFCs. The objectives of this study include the synthesis of carbon support materials, deposition of Pt onto the support material, physical characterisation of the catalysts, determination of their activity, and utilisation of the catalysts in a PEMFC.

The different synthesis methods of depositing Pt nanoparticles onto PDC by using $NaBH_4$ (**NBH**), ethylene glycol (**EG1**, **EG2**, **EG3**, **EG4**), or isopropyl alcohol (**IPA**) as a reducing agent were successful. XRD analysis indicated the presence of Pt in all catalyst materials. The Pt content of the synthesised catalysts was approximately 60% based on TGA results. The Pt crystallite sizes of the materials were determined by XRD measurements ranging from 2.4 (**EG1**) to 6 nm (**IPA**). N_2 sorption analysis showed that the synthesised materials were micro-mesoporous. SEM images of the materials were taken to inspect the morphology of the synthesised catalyst materials. From the SEM-EDX analysis, it was determined that the composition of synthesised catalyst materials was mostly platinum and carbon.

The studied catalyst materials were characterised electrochemically using various electrochemical methods. ECSA was measured in both a three-electrode system in 0.1 M $HClO_4$ solution and in a PEMFC single cell. The ORR kinetics of the materials were studied with the RDE method. The RDE and PEMFC single cell measurements revealed that the ECSA value strongly impacts the catalytic activity of the catalyst. The smaller the Pt crystallite size of the material, the larger the ECSA values, and the higher the catalytic activity. For optimal PEMFC unit cell measurements different MEA suspension coating methods were tested. It was found that the best coating method, for the synthesised materials, was to pipette the suspension dropwise directly onto the GDL. This formed a porous catalyst layer, with good mass transport properties. Also, adding different dimensional carbon materials to the PEMFC catalyst layer proved to be an effective way to improve fuel cell performance. The maximum power density of **EG3**, initially 0.45 W cm^{-2}, was increased to 0.53 W cm^{-2} (**EG3 + KB**).

The power and current density of the materials were compared to a commercial catalyst material. The ORR activity of the materials measured in a three-electrode system decreased in order: 60% Pt on HSA Ketjenblack (MA = 284 A g^{-1}_{Pt}) > **EG4** (MA = 278 A g^{-1}_{Pt}) > **EG3** > **EG1** > **EG2** > **IPA** > **NBH**. The ORR activity of the RDE measurements of material **EG4** is comparable to the commercial material. However, in a PEMFC the studied materials were less active than the commercial material. Further development is needed to achieve the activity of a commercial catalyst in a PEMFC.

References

[1] Parlament kinnitas kliimaseaduse. https://www.europarl.europa.eu/news/et/press-room/20210621IPR06627/parlament-kinnitas-kliimaseaduse-2050-aastaks-peab-el-olema-kliimaneutraalne (last accessed: 23.05.2023)

[2] M.H. Esfe, M. Afrand, *J. Therm. Anal. Calorim.* 140 (2020) 1633.

[3] R.K. Pachauri, Y.K. Chauhan, *Renew. Sust. Energ. Rev.* 43 (2015) 1301.

[4] O.Z. Sharaf, M.F. Orhan, *Renew. Sust. Energ. Rev.* 32 (2014) 810.

[5] Y. Wang, K.S. Chen, J. Mishler, S.C. Cho, X.C. Adroher, *Appl. Energ.* 88 (2011) 981.

[6] Frano Barbir, PEM Fuel Cells. Theory and Practice, 2nd ed., Elsevier Inc., Amsterdam, Boston, 2013, pp. 1-518.

[7] S. Sharma, B.G. Pollet, *J. Power Sources* 208 (2012) 96.

[8] M. Ji, Z. Wei, *Energies* 2 (2009) 1057.

[9] R. Othman, A.L. Dicks, Z. Zhu, *Int. J. Hydrogen Energ.* 37 (2012) 357.

[10] S. Akula, M. Mooste, B. Zulevi, S. McKinney, A. Kikas, H.-M. Piirsoo, M. Rähn, A. Tamm, V. Kisand, A. Serov, E.B. Creel, D.A. Cullen, K.C. Neyerlin, H. Wang, M. Odgaard, T. Reshetenko, K. Tammeveski, *J. Power Sources* 520 (2022) 230819.

[11] F.D. Sanij, P. Balakrishnan, P. Leung, A. Shah, H. Su, Q. Xu, *Int. J. Hydrogen Energ.* 46 (2021) 14596.

[12] E. Antolini, *Appl. Catal. B-Environ.* 88 (2009) 1.

[13] S. Samad, K.S. Loh, W.Y. Wong, T.K. Lee, J. Sunarso, S.T. Chong, W.R. Wan Daud, *Int. J. Hydrogen Energ.* 43 (2018) 7823.

[14] Y.-J. Wang, B. Fang, H. Li, X.T. Bi, H. Wang, *Prog. Mater. Sci.* 82 (2016) 445.

[15] Y. Lin, J. Yu, X. Zhang, J. Fang, G.-P. Lu, H. Huang, *Chinese Chem. Lett.* 33 (2022) 186.

[16] H. Jinming, M. Xuehui, Physical and Chemical Properties of Peat in: G. Jinsheng (Eds.), Coal, Oil Shale, Natural Bitumen, Heavy Oil and Peat, Vol. 2, UNESCO-EOLSS, 2011, pp. 309–326.

[17] M. Härmas, R. Palm, T. Thomberg, R. Härmas, M. Koppel, M. Paalo, I. Tallo, T. Romann, A. Jänes, E. Lust, *J. Appl. Electrochem.* 50 (2020) 15.

[18] A. Adamson, R. Väli, M. Paalo, J. Aruväli, M. Koppel, R. Palm, E. Härk, J. Nerut, T. Romann, E. Lust, A. Jänes, *RSC Adv.* 10 (2020) 20145.

[19] P. Teppor, R. Jäger, M. Paalo, A. Adamson, M. Härmas, O. Volobujeva, J. Aruväli, R. Palm, E. Lust, *Int. J. Hydrogen Energ.* 47 (2022) 16908.

[20] K. Shinozaki, J.W. Zack, S. Pylypenko, B.S. Pivovar, S.S. Kocha, *J. Electrochem. Soc.* 162 (2015) F1384.

[21] C. Du, Q. Tan, G. Yin, J. Zhang, Rotating Disk Electrode Method in: W. Xing, G. Yin, J. Zhang (Ed.), Rotating Electrode Methods and Oxygen Reduction Electrocatalysts, Elsevier, Amsterdam, 2014, pp. 171–198.

[22] J. Zhang, ed., PEM Fuel Cell Electrocatalysts and Catalyst Layers, Springer London, London, 2008, pp. 1-1137.

[23] S. Srinivasan, Fuel Cells: From Fundamentals to Applications, Springer Science & Business media, Boston, 2006, pp. 1-691.

[24] A.J. Bard, L.R. Faulkner, Electrochemical Methods: Fundamentals and Applications, 2nd ed., Wiley, New York, 2001, pp. 1-736.

[25] N.M. Markovic, H.A. Gasteiger, P.N. Ross, *J. Phys. Chem.* 99 (1995) 3411.

[26] M.K. Debe, *Nature* 486 (2012) 43.

[27] Z. Li, Z. Zheng, L. Xu, X. Lu, *BMC Energy* 1 (2019).

[28] S. Sepp, Influence of Porosity of the Carbide-Derived Carbon on the Properties of the Composite Electrocatalysts and Characteristics of Polymer Electrolyte Fuel Cells, PhD Thesis, Tartu, 2016. https://dspace.ut.ee/handle/10062/55070 (last accessed: 23.05.2023)

[29] J. Luna, E. Usai, A. Husar, M. Serra, in: IECON 2016 - 42nd Annual Conference of the IEEE Industrial Electronics Society, IEEE, Florence, Italy, 2016, pp. 5483–5488. http://ieeexplore.ieee.org/document/7793321 (last accessed: 23.05.2023)

[30] S. Trasatti, O.A. Petrii, *J. Electroanal. Chem.* 327 (1992) 353.

[31] T. Biegler, D.A.J. Rand, R. Wood, *J. Electroanal. Chem.* 29 (1971) 269.

[32] K. Shinozaki, J.W. Zack, R.M. Richards, B.S. Pivovar, S.S. Kocha, *J. Electrochem. Soc.* 162 (2015) F1144.

[33] S. Sepp, K. Vaarmets, J. Nerut, I. Tallo, E. Tee, H. Kurig, J. Aruväli, R. Kanarbik, E. Lust, *Electrochim. Acta* 203 (2016) 221.

[34] K. Vaarmets, P. Valk, J. Nerut, I. Tallo, J. Aruväli, S. Sepp, E. Lust, *ECS Trans.* 80 (2017) 743.

[35] P. Valk, J. Nerut, R. Kanarbik, I. Tallo, J. Aruväli, E. Lust, *J. Electrochem. Soc.* 165 (2018) F315.

[36] R. Kou, Y. Shao, D. Mei, Z. Nie, D. Wang, C. Wang, V.V. Viswanathan, S. Park, I.A. Aksay, Y. Lin, Y. Wang, J. Liu, *J. Am. Chem. Soc.* 133 (2011) 2541.

[37] Y. Shao, S. Zhang, R. Kou, X. Wang, C. Wang, S. Dai, V. Viswanathan, J. Liu, Y. Wang, Y. Lin, *J. Power Sources* 195 (2010) 1805.

[38] M. Inaba, J. Quinson, J.R. Bucher, M. Arenz, *J. Vis. Exp.* (2018) 57105.

[39] J. Quinson, M. Inaba, S. Neumann, A.A. Swane, J. Bucher, S.B. Simonsen, L. Theil Kuhn, J.J.K. Kirkensgaard, K.M.Ø. Jensen, M. Oezaslan, S. Kunz, M. Arenz, *ACS Catal.* 8 (2018) 6627.

[40] L. Cui, J. Zhang, H. Wang, S. Lu, Y. Xiang, *Int. J. Hydrogen Energ.* 46 (2021) 15887.

[41] M. Uchida, Y. Aoyama, N. Eda, A. Ohta, *J. Electrochem. Soc.* 142 (1995) 4143.

[42] M. Uchida, Y. Fukuoka, Y. Sugawara, N. Eda, A. Ohta, *J. Electrochem. Soc.* 143 (1996) 2245.

[43] Particle size analyzer manual. https://eng.auburn.edu/files/acad_depts/matl/lab-manuels/261%20-%20Analytical%20Lab/manuals/particle-size-analyzer-manual.pdf (last accessed: 23.05.2023)

[44] J. Jagiello, J.P. Olivier, *Carbon* 55 (2013) 70.

[45] J. Jagiello, J.P. Olivier, *Adsorption* 19 (2013) 777.

[46] M. Gara, K.R. Ward, R.G. Compton, *Nanoscale* 5 (2013) 7304.

[47] M.B. Sassin, Y. Garsany, B.D. Gould, K.E. Swider-Lyons, *Anal. Chem.* 89 (2017) 511.

[48] S.A. Mauger, J.R. Pfeilsticker, M. Wang, S. Medina, A.C. Yang-Neyerlin, K.C. Neyerlin, C. Stetson, S. Pylypenko, M. Ulsh, *J. Power Sources* 450 (2020) 227581.

[49] J. Rouquerol, D. Avnir, C.W. Fairbridge, D.H. Everett, J.M. Haynes, N. Pernicone, J.D.F. Ramsay, K.S.W. Sing, K.K. Unger, *Pure Appl. Chem.* 66 (1994) 1739.

[50] J.W. Arblaster, *Platin. Met. Rev.* 50 (2006) 118.

[51] I.N. Leontyev, A.B. Kuriganova, N.G. Leontyev, L. Hennet, A. Rakhmatullin, N.V. Smirnova, V. Dmitriev, *RSC Adv.* 4 (2014) 35959.

[52] T. Shinagawa, A.T. Garcia-Esparza, K. Takanabe, *Sci. Rep.* 5 (2015) 13801.

[53] Y. Garsany, I.L. Singer, K.E. Swider-Lyons, *J. Electroanal. Chem.* 662 (2011) 396.

[54] M. Prasanna, H.Y. Ha, E.A. Cho, S.-A. Hong, I.-H. Oh, *J. Power Sources* 137 (2004) 1.

[55] F. Jaouen, V. Goellner, M. Lefèvre, J. Herranz, E. Proietti, J.P. Dodelet, *Electrochim. Acta* 87 (2013) 619.

[56] S. Ott, F. Du, M.L. Luna, T.A. Dao, B.R. Cuenya, A. Orfanidi, P. Strasser, *J. Electrochem. Soc.* 169 (2022) 054520.

Acknowledgments

The author thanks his supervisors, Jaak Nerut and Heili Kasuk. The author would also like to thank Anu Adamson for synthesising the peat-derived carbon, Thomas Thomberg for his help in reducing the carbon materials with hydrogen, Jaan Aruväli for performing X-ray diffraction analysis, Peeter Valk for his assistance with Pt deposition and particle size measurements, Olga Volobujeva for SEM and SEM-EDX analysis (TalTech), and Miriam Koppel and Patrick Teppor for their help in measuring low-temperature N_2 sorption. The author expresses gratitude towards the Chair of Physical Chemistry and Professor Enn Lust.

The author acknowledges the financial support from the European Union Regional Development Fund project TK141 “Innovative materials and high-tech equipment for energy recovery systems” (2014-2020.4.01.15-0011), the Estonian Research Agency project (personal research support group grant project No. PRG676)), and the Estonian Energy Technology Program: SLOKT10209T “Nanomaterials – research and applications (NAMUR)” project 3.2.0304.12-0397. The author also expresses thanks to the private limited company AuVe Tech (research and development project LLTKT20148 “Production of Polymer Electrolyte Membrane Fuel Cell”).

Appendices

Appendix 1. Some examples of optical microscope images of the glassy carbon electrodes covered with different catalyst materials.

Figure 1. Optical microscope image of a glassy carbon electrode covered with **IPA**.

Figure 2. Optical microscope image of a glassy carbon electrode covered with **NBH**.

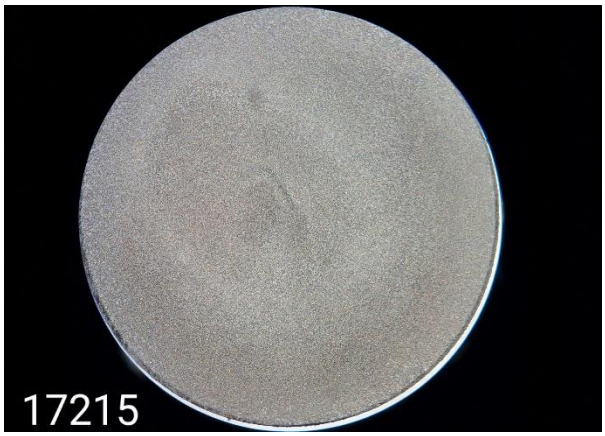

Figure 3. Optical microscope image of a glassy carbon electrode covered with **EG1**.

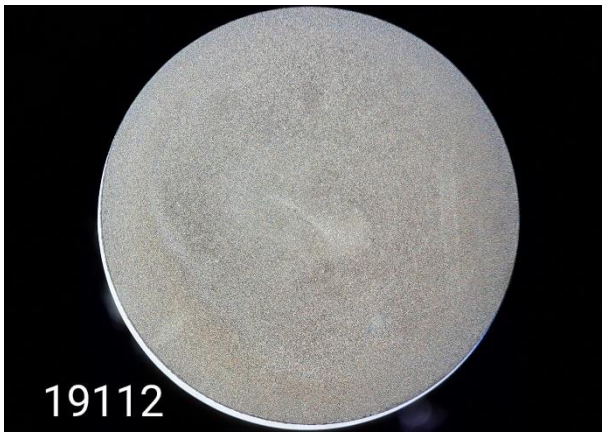

Figure 4. Optical microscope image of a glassy carbon electrode covered with **EG2**.

Appendix 2.

Wiljar Lobjakas, Jaak Nerut, Heili Kasuk, Anu Adamson, Thomas Thomberg, Jaan Aruväli, Peeter Valk, Patrick Teppor, Miriam Koppel, Valdek Mikli, Olga Volobujeva, Enn Lust

Investigation of Oxygen Reduction on Platinum Nanoparticles Deposited Onto Peat-Derived Carbon Carrier
ECS Transactions 108 (2022) 49−58.

ECS Transactions, 108 (7) 49-58 (2022)
10.1149/10807.0049ecst ©The Electrochemical Society

Investigation of Oxygen Reduction on Platinum Nanoparticles Deposited Onto Peat-Derived Carbon Carrier

Wiljar Lobjakas[a,*], Jaak Nerut[a], Heili Kasuk[a], Anu Adamson[a], Thomas Thomberg[a], Jaan Aruväli[b], Peeter Valk[a], Patrick Teppor[a], Miriam Koppel[a], Valdek Mikli[c], Olga Volobujeva[c], Enn Lust[a]

[a]Institute of Chemistry, University of Tartu, 50411, Estonia
[b]Institute of Ecology and Earth Sciences, University of Tartu, 50411, Estonia
[c]Department of Materials and Environmental Technology, Tallinn University of Technology, 12616, Estonia

Carbon supported platinum catalysts for proton exchange membrane fuel cell (PEMFC) applications have been studied intensively in the scientific community. The aim of this study was to investigate the oxygen reduction reaction (ORR) on platinum nanoparticles deposited onto peat-derived carbon. The Pt nanoparticles were deposited onto the carbon support material by three different methods – using $NaBH_4$ (NBH), ethylene glycol (EG) or isopropyl alcohol (IA) as a reducing agent. The structure of the studied materials was characterized using N_2 sorption analysis, X-ray diffraction analysis, thermogravimetric analysis and scanning electron microscopy with energy-dispersive X-ray analysis methods. For electrochemical characterization, the electrochemically active surface area (ECA) and the ORR kinetics of the materials were measured in a PEMFC. The catalytic activity of the synthesized materials depends on the Pt reduction method and increases in order: IA < NBH < EG. It was found that materials with high ECA also have high catalytic activity.

Introduction

Carbon supported platinum catalysts for proton exchange membrane fuel cell (PEMFC) applications have been studied intensively in the scientific community (1). The catalytic activity of the catalyst depends on the characteristics of the supporting material (usually carbon) (2). Precious metal catalysts (usually platinum) deposited onto a support material are used to catalyze the oxygen reduction reaction (ORR) taking place in a PEMFC (3). Many different carbon materials have been studied as support materials for Pt. Still, there is only a limited amount of data regarding peat-derived carbon (PDC) as a catalyst support material (4).

The aims of this study were: 1) to synthesize a PDC support material and use it as catalyst support for the Pt catalyst materials synthesized using three different methods: reduction with $NaBH_4$, reduction with isopropyl alcohol, and microwave-assisted synthesis using ethylene glycol as a reducing agent, 2) to conduct a structural characterization of the synthesized materials using N_2 sorption analysis, X-ray diffraction analysis (XRD), thermogravimetric analysis (TGA) and scanning electron microscopy with energy-

dispersive X-ray analysis (SEM-EDX), and 3) to study the activity of the Pt-C materials in a PEMFC single cell.

Experimental

Synthesis of carbon support material

Highly decomposed peat was collected from Möllatsi bog in Estonia. The PDC was prepared using the following three steps. Firstly, the peat was washed with water (MilliQ$^+$), then homogenized and pre-pyrolyzed for 3 h at 450 °C. Secondly, the obtained carbonaceous material was alkali/acid-treated (stirred for 2 h in 20 % KOH at 70 °C, then 50 % HCl solution was added until the pH reached ~1). The carbonaceous material was rinsed with water (MilliQ$^+$) and dried in a vacuum oven (80 mbar, 100 °C) to remove residues. As a final step, the carbonaceous material was post-pyrolyzed at 800 °C. (5)

Thereafter, the carbon material was milled in a planetary mill (FRITSCH Pulverisette 6) for 2 hours and 15 minutes at 350 rpm to reduce the particle size, and finally reduced with hydrogen for 2 h at 800 °C to remove functional groups in the carbon material (-OH, -COOH, -CHO, etc.).

Synthesis of the catalysts

For the first catalyst material (NBH), the Pt-nanoparticles were deposited onto the carbon support using the sodium borohydride reduction method (6). The required amount of $H_2PtCl_6{\times}6H_2O$ (Alfa Aesar, 99.9 %) was dissolved in of MilliQ$^+$ water to prepare a solution with a Pt-compound concentration of ~1 mM. The prepared solution was stirred at room temperature for 45 min. 20 wt% NaOH was added until the pH of the solution reached ~8. The required quantity of PDC was added to the H_2PtCl_6 solution. After that, 1 M $NaBH_4$ (Aldrich Chemistry, 98.0 %) solution was prepared and added drop-wise to the previously prepared suspension. The reaction mixture was stirred for 2 h and left to settle overnight. The catalyst was filtered, rinsed and dried in a vacuum oven at 50 mbar and 110 °C.

For the second catalyst material (EG), the Pt-nanoparticles were deposited onto the carbon support by the microwave-assisted ethylene glycol reduction method (7). The required amount of $H_2PtCl_6{\times}6H_2O$ (Alfa Aesar, 99.9 %) was dissolved in 1 cm^3 of MilliQ$^+$ water, and the carbon was added. 60 cm^3 of ethylene glycol (EMSURE, 99.5 %) was added, and the pH was regulated by adding 20 wt% NaOH (Pt:Na molar ratio 1:10). The mixture was sonicated for 1 h (37 kHz, 100 %). The suspension was heated using a commercial 750 W microwave for 80 s. After cooling, 500 cm^3 of MilliQ$^+$ water was added, and the mixture was stirred overnight. The catalyst prepared was filtered, rinsed, and dried in a vacuum oven at 50 mbar and 100 °C.

For the third catalyst material (IA), the Pt-nanoparticles were deposited onto the carbon support by the isopropyl alcohol reduction method. The required amount of $H_2PtCl_6{\times}6H_2O$ (Alfa Aesar, 99.9 %) was weighed, and 12 cm^3 of isopropyl alcohol (J. T. Baker, 99.5 %) was added. The mixture was sonicated for 1 min (37 kHz, 100 %). In a second vial with the required quantity of carbon, the previously prepared Pt-compound mixture was added

in three portions of 4 cm^3. After adding each portion, the mixture was sonicated for 30 min (37 kHz, 100 %), then dried in an oven at 85 °C until the isopropyl alcohol had evaporated, and crushed into a powder.

Methods of structural characterization

Particle size distribution was determined by a MICROTRAC S3500 Model Bluewave particle size analyzer using the dynamic light scattering method. Isopropyl alcohol (J. T. Baker, 99.5 %) was used as a solvent for PDC.

The porosity and specific surface area of the materials were evaluated by using the low-temperature (−195.8 °C) N_2 sorption method with a Micromeritics ASAP 2020 instrument. Adsorption isotherms were analyzed with SAIEUS software, using a two-dimensional non-local density functional theory (2D-NLDFT). The specific surface area (S_{DFT}) and pore volume (V_{DFT}) were calculated according to 2D-NLDFT approximations. In addition, the specific surface area (S_{BET}) was calculated according to the Brunauer-Emmett-Teller (BET) theory. The total pore volume (V_{tot}) was estimated at a pressure close to the saturation pressure ($p\,p_0^{-1} = 0.95$). (8)

The XRD patterns for studied materials were collected with a Bruker D8 Advance diffractometer with Ni filtered CuK_α radiation (0.6 mm wide parallel beam, two 2.5° Soller slits and LynxEye line detector system). The scanning step of 0.01° for 2θ was applied from 10° to 90° and the total counting time per step was 166 s. The operating voltage of the X-ray tube was 40 kV, and the current was 40 mA. (9)

The content of Pt in the catalysts was determined by TGA, using NETZSCH STA 449 F3 Jupiter instrument. Measurements were performed at a temperature from 25 °C to 800 °C. The heating rate was 10 °C min^{-1}, and the synthetic air flow rate was 50 cm^3 min^{-1}. The sample weight was approximately 10 mg. The synthetic air contained 80 % nitrogen (5.0, Linde Gas) and 20 % oxygen (5.0, Linde Gas).

SEM-EDX examination was conducted using Zeiss ULTRA 55 SEM. The sample was prepared on charcoal tape. The sample chamber was under high vacuum conditions. The InLens SEM images of the materials were taken with different magnifications using signals of secondary electrons. The composition of the sample was determined using EDX analysis.

Membrane electrode assembly preparation

The catalyst materials were suspended in a mixture of MilliQ$^+$ water, Nafion solution (D521 Nafion^{TM} Solution, Ion Power, 5 %) and isopropyl alcohol (10). The mixture was stirred (4 h, 14600 rpm) using a HIGH-SHEAR T10 or T25 IKA Ultra mixer to obtain a homogeneous suspension. The suspension was mixed overnight using a magnetic stirrer at 750 rpm, and before deposition, the suspension was sonicated for 15 min (37 kHz, 100 %) and stirred with HIGH-SHEAR mixer for 1 h at 14600 rpm.

For the PEMFC measurements, 5 cm^2 membrane electrode assemblies (MEA) were prepared (10). The suspension was pipetted onto a gas diffusion layer Freudenberg H23C3 Carbon Paper (FuelCellStore) to make the cathode. For the anode, a commercial catalyst (60 % Pt on HSA Ketjenblack) suspension was deposited onto a Nafion membrane

(NAFION^{TM} Membrane HP, Ion Power) using an ultrasonic coating system Sono-Tek ExactaCoat. The loading of catalyst material for anode was 0.5 mg cm^{-2} and for cathode 0.7 mg cm^{-2}.

Methods of electrochemical measurements

The measurements were conducted in a 5 cm^2 PEMFC single cell. Autolab PGSTAT 302N with FRA32M and a BOOSTER20A, using Nova software, were used. To control the gas flow rate and humidity, a FUEL CELL TECHNOLOGIES INC. instrument was used. The cell temperature was 62 °C, the temperature of the humidification vessels and the gas line was 60 °C. Gas applied to the anode was H_2 (5.0, Linde Gas), the flow rate was 200 cm^3 min^{-1} at a pressure of 1.4 bar. Gas applied to the cathode side was air (Linde Gas, Airapy: O_2 21.5 %, N_2 78.5 %), the flow rate was 2 dm^3 min^{-1} at atmospheric pressure. After the cell reached measurement conditions, it was cycled between open circuit voltage (OCV) and 0.4 V. After cycling, potential in the current range from 0 A to the maximum current was measured in 0.2 A steps (dependence of current on the cell voltage and power was obtained).

The single cell and humidification vessels were at room temperature for the electrochemically active surface area (ECA) evaluation. H_2 was applied to the anode at atmospheric pressure, and the gas flow rate was 12 cm^3 min^{-1}. N_2 (5.0, Linde Gas) was applied to the cathode at atmospheric pressure, and the gas flow rate was 200 cm^3 min^{-1}. The current-voltage data were measured in the potential range from 0.08 V to 1.00 V at potential scan rates from 20 mV s^{-1} to 300 mV s^{-1}.

Results and Discussion

Structural characteristics of the materials

The influence of milling on the particle size distribution is shown in Figure 1. The milling reduced the size of the PDC particles by one order of magnitude. Milling of the carbon was necessary to prepare a time-stable suspension for electrode preparation.

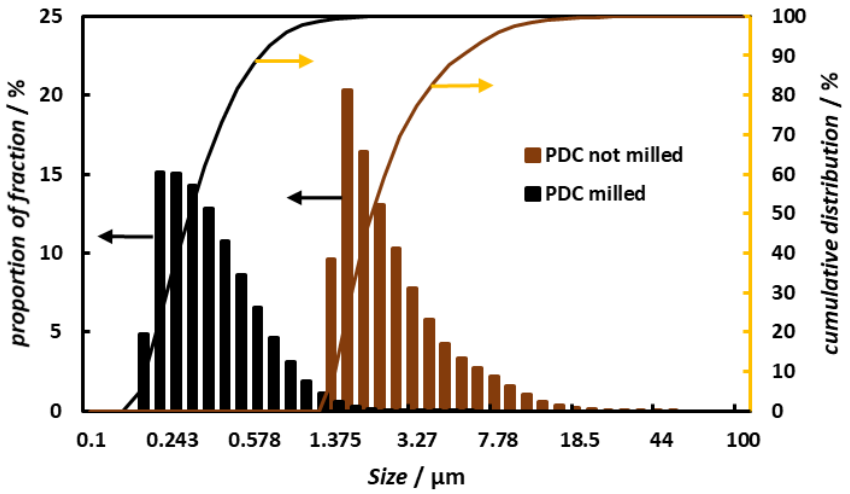

Figure 1. Particle size distribution of PDC before and after milling.

The results of N_2 sorption measurements are shown in Table I. According to the BET theory, all pores accessible to N_2 were taken into account in calculating the specific surface area. The pore distributions calculated by the 2D-NLDFT mainly describe micropores, as pores larger than 30 nm are not taken into account. Therefore the amount of micropores may be somewhat overestimated (8). The pore size distribution data for the materials are shown in Figure 2. All synthesized materials are micro-mesoporous. Precipitation of Pt onto PDC decreased the proportion of micropores, which can be explained by the deposition of platinum into the micropores. The specific surface area of the investigated Pt-C materials prepared using various reduction methods increased in order: IA < NBH <EG.

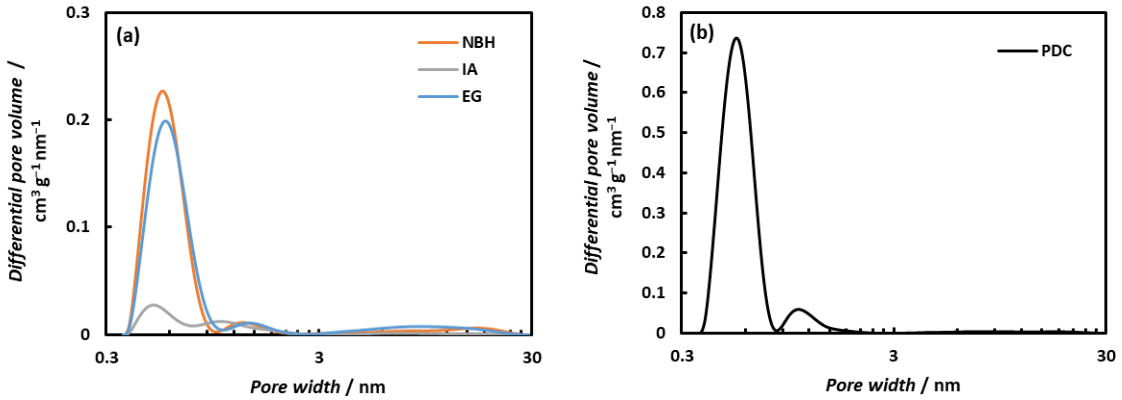

Figure 2. The pore distribution of the investigated Pt-C materials (a) and the corresponding carbon support material (b).

TABLE I. Results of N_2 sorption measurements.

Material	S_{BET} / $m^2\ g^{-1}$	S_{DFT} / $m^2\ g^{-1}$	S_{micro} / $m^2\ g^{-1}$	V_{tot} / $cm^3\ g^{-1}$	V_{DFT} / $cm^3\ g^{-1}$	V_{micro} / $cm^3\ g^{-1}$
PDC	420	660	646	0.25	0.25	0.19
NBH	170	240	226	0.17	0.16	0.07
IA	40	40	40	0.04	0.04	0.02
EG	170	230	210	0.19	0.18	0.23

S_{BET} – multi point BET surface area, S_{DFT} – 2D-NLDFT surface area, S_{micro} – micropore area, V_{micro} – micropore volume, V_{tot} – total pore volume, V_{DFT} – 2D-NLDFT pore volume.

The collected XRD data are presented in Figure 3. The characteristic Pt reflexes are very clearly visible, corresponding to the Pt(111), Pt(200), Pt(220), Pt(311) and Pt(222) planes (12). The carbon support materials also have distinguishable characteristic reflexes, corresponding to planes C(002) and C(100/101) (13). In the case of PDC material, reflexes of quartz, silicates and iron compounds are visible because the source material (peat) comes from nature, and some impurities remain inside of the carbon material prepared. PDC also had ZrO_2 and titanate reflexes These compounds were most likely introduced into the carbon material the during milling step.

Full profile analysis was conducted using TOPAS software to calculate the lattice parameters and the size of Pt crystallites. The results are shown in Table II. The lattice parameter for the studied materials varies between 3.91 and 3.92 Å. This is less than, $a = 3.9236 \pm 0.0006$ Å, reported in the literature (14). The literature has shown that when the size of the platinum crystallite is small, the lattice parameter decreases (15). The result

obtained can therefore be considered reasonable. The Pt crystallite size increases in order EG < NBH < IA.

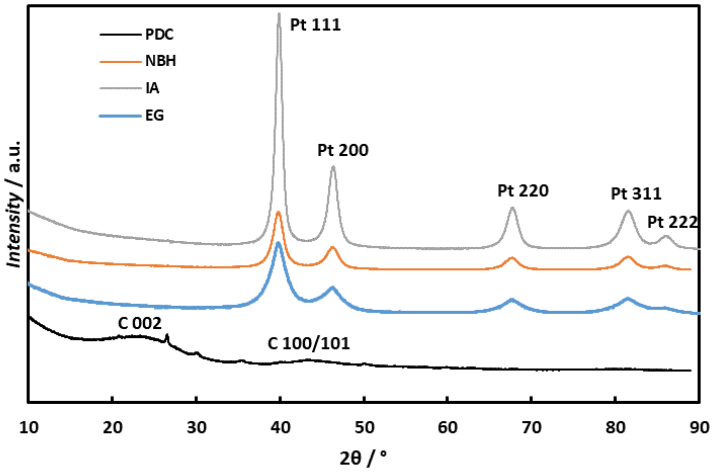

Figure 3. X-ray diffraction patterns of the studied materials.

TABLE II. Pt crystallite size, d_{Pt}, lattice parameter, a, and Pt content of the synthesized catalyst materials.

Material	Pt crystallite size d_{Pt} / nm	Lattice parameter a / Å	Pt content / wt%
NBH	4.0	3.915 ± 0.001	60.4
IA	6.0	3.916 ± 0.001	58.6
EG	2.4	3.920 ± 0.011	59.1

TGA was used to determine the content of Pt in the synthesized materials and assess the thermal stability of the materials. TGA results are shown in Figure 4. The significant weight loss between 300 °C and 500 °C corresponds to the oxidation of carbon. The content of Pt in the catalyst material was calculated using the weight losses of the PDC support and the Pt-C materials. The calculated wt% of Pt in the catalyst materials are shown in Table II. The Pt concentrations calculated from TGA results confirm that catalyst materials with 60 wt% Pt content were synthesized. The temperature at which the weight of the Pt-C materials reached 80 wt% increases in order: EG < NBH < IA. This correlates to the Pt crystallite size, d_{Pt}, which increases in the same order. This shows that PDC for Pt-C materials with larger d_{Pt} react with oxygen at higher temperatures, making them thermally more stable (although less active).

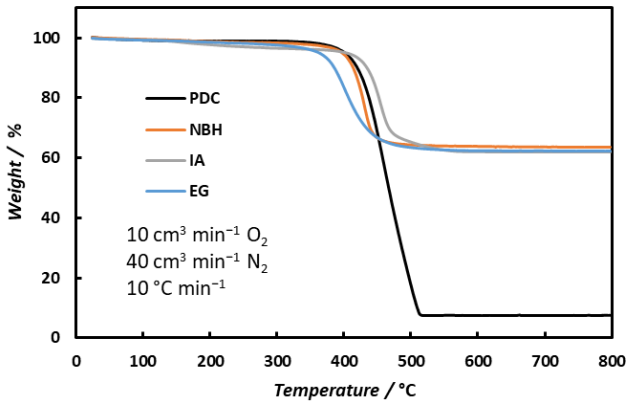

Figure 4. Thermogravimetry of the studied materials.

SEM images for all Pt-C materials under study are shown in Figure 5. The effects of milling are seen in Figure 5a. The dimensions of the carbon support particles measured directly from SEM are under 1 μm (Figure 1). A porous structure can be observed, Pt particles (white) are deposited inside the opened pores. SEM image of the synthesized EG material is shown in Figure 5b; it can be seen that the Pt nanoparticles have uniformly dispersed onto/into the carbon particles forming a "web-like" structure. For comparison, Figure 5c shows SEM images of NBH material, the Pt particles are more agglomerated and not as well dispersed. In Figure 5d, large round Pt nanoclusters can be seen. The IA material is not evenly covered by Pt nanoparticles at all. This is in accord with XRD data (Table II) that gives Pt crystallite sizes of the materials increasing in order: EG < NBG < IA. This also correlates to N_2 sorption data (Table I). IA material with large Pt nanoclusters has a significantly smaller specific surface area than EG and NBH.

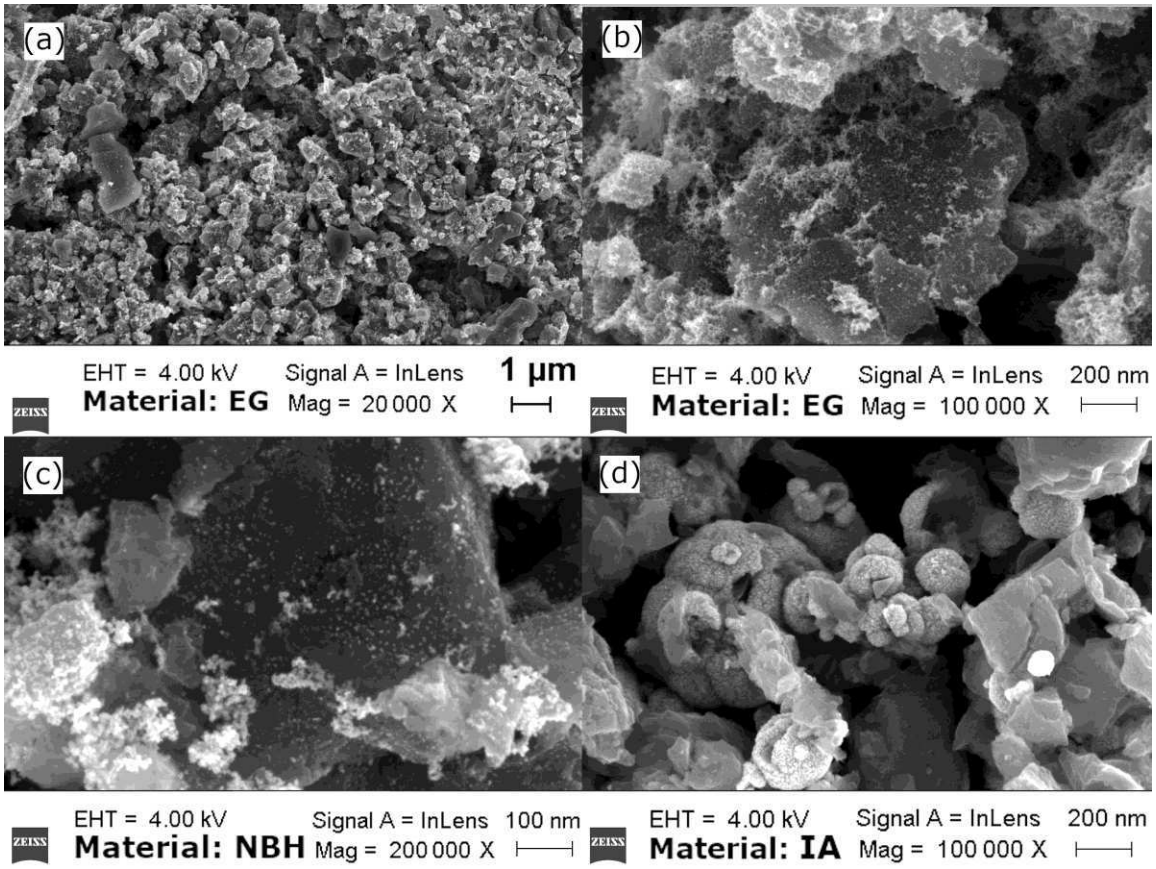

Figure 5. SEM images of the synthesized Pt-C materials.

EDX data were used to confirm the chemical composition of the synthesized Pt-C materials. The EDX analysis showed that all synthesized catalyst materials contain carbon, oxygen and platinum. The EDX data did reveal the existence of impurities in the materials, except small amounts of silicon and chlorine.

The electrochemical measurements

The dependence of calculated gravimetric capacitance on potential, for the synthesized materials in PEMFC single cell, are shown in Figure 6. ECA values were calculated from the data in the graph (16). The different characteristic regions are visible. The hydrogen

adsorption-desorption peaks in the potential range from 0.31 V to 0.35 V, the oxidation of Pt particles and the subsequent reduction back to Pt from 0.65 V to 1.00 V and the electrical double-layer (EDL) area are visible. All Pt-C materials have a relatively large gravimetric capacitance in the EDL region. The large capacity in the EDL area indicates that the Nafion chains are probably in good contact with the catalyst support particles.

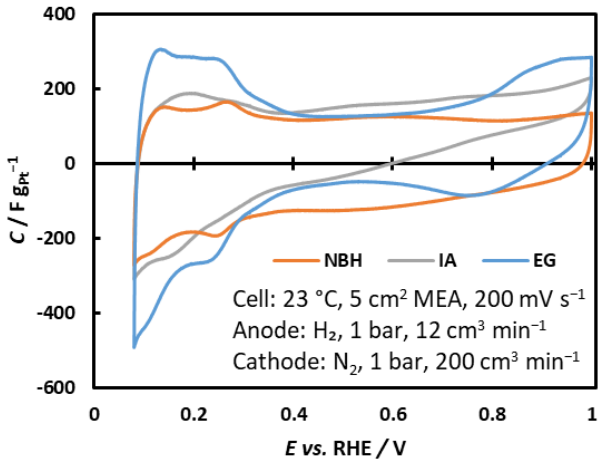

Figure 6. Dependence of the calculated gravimetric capacitance on the potential for the synthesized materials in PEMFC single cell measurements.

The calculated ECA values and the results of PEMFC single cell measurements are shown in Table III. The material with the highest ECA (EG) of 22 $m_{Pt}^2\ g_{Pt}^{-1}$ also has the smallest medium Pt crystallite size value, d_{Pt} = 2.4 nm (Table II). Material EG also shows the highest catalytic activity of the synthesized materials. Materials with lower ECA values of 9.5 $m_{Pt}^2\ g_{Pt}^{-1}$ and 6.2 $m_{Pt}^2\ g_{Pt}^{-1}$ were IA and NBH, respectively. There is a correlation between the Pt crystallite size and the ECA value. A material with a small d_{Pt} value demonstrates larger ECA values. This does not apply to materials with large Pt agglomerates. The correlation is also influenced by the location of Pt particles. Probably, the ionomer chains do not reach the Pt nanoparticles located deep inside of the pores of the carbon support material. Therefore, those Pt particles do not contribute to the catalytic activity. NBH material has a smaller Pt crystallite size and a lower ECA value than IA material. However, NBH material showed higher catalytic activity. This may be due to the optimal structure of NBH and unfavorable structure of the IA material. The Pt nanoparticles are agglomerated into large clusters (Figure 5d), making the reagents and ionomer chains inaccessible to the entire Pt catalyst.

TABLE III. Results of the PEMFC single cell measurements.

Material	*ECA* / $m_{Pt}^2\ g_{Pt}^{-1}$	*OCV* / mV	*j* at 700mV / A cm^{-2}	P_{max} / W cm^{-2}	*R* at −450 mV / mΩ
NBH	6.2	954	0.186	0.235	12.3
IA	9.5	633	-	0.028	-
EG	22	882	0.426	0.421	9.6

ECA – electrochemically active surface area of platinum, *OCV* – open circuit voltage, *j* – current density, P_{max} – maximum power density, *R* – resistance.

PEMFC single cell measurement results for the Pt-C materials are shown in Figure 7. It was found that the higher the ECA value of the material, the higher the catalytic activity

of the catalyst material. The highest catalytic activity was measured in the case of the EG material, at 700 mV $j = 0.426$ A cm^{-2} and $P_{max} = 0.421$ W cm^{-2}. The synthesis of the EG material took place in the suspension phase. As a result, Pt nanoparticles dispersed onto/into the carbon support more uniformly (Figure 5) and with a smaller crystallite size (Table II) than in the syntheses of IA (paste phase) and NBH (solution phase) materials. The maximal power of PEMFC single cells based on prepared materials increase in order: IA < NBH <EG.

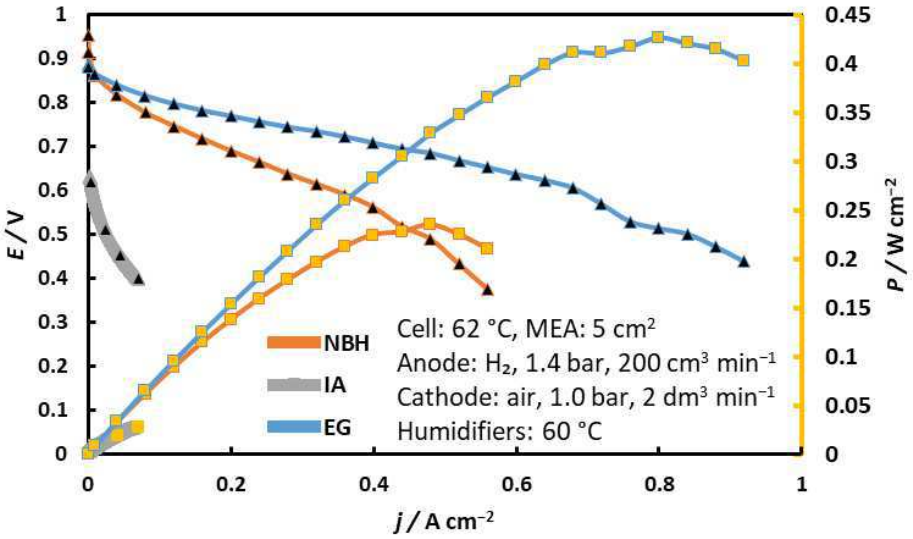

Figure 7. PEMFC single cell measurement results of the Pt-C materials. Dependence of cell voltage (triangles) and power density (squares) on current density applied.

Conclusion

The Pt-C catalyst materials were synthesized by depositing Pt onto PDC support material with three different chemical reduction synthesis methods. N_2 sorption analysis showed that the synthesized materials were micro-mesoporous. XRD analysis indicated the presence of Pt in all synthesized Pt-C materials, and the Pt crystallite sizes were determined by a full profile analysis method. Based on the TGA results, the Pt content for all synthesized Pt-C materials was calculated to be approximately 60 wt%. SEM images of the materials were taken to inspect the morphology of the synthesized catalyst materials. From the SEM-EDX analysis, it was determined that the composition of all synthesized catalyst materials was mostly carbon and platinum.

The electrochemical characteristics for the catalyst materials were studied in a PEMFC single cell. The highest catalytic activity (at 700mV $j = 0.426$ A cm^{-2} and $P_{max} = 0.421$ W cm^{-2}) and ECA value (22 m_{Pt}^2 g_{Pt}^{-1}) was observed for the EG material, synthesized using a microwave-assisted synthesis method and ethylene glycol as a reducing agent. As a result, the Pt nanoparticles were dispersed onto/into the PDC support material more uniformly and with a smaller crystallite size ($d_{Pt} = 2.4$ nm) than in the syntheses of IA and NBH materials.

Acknowledgments

The author thanks the European Union Regional Development Fund for the financial support of the project TK141 "Innovative materials and high-tech equipment for energy recovery systems" (2014-2020.4.01.15-0011); the Estonian Research Agency project (personal research support group grant project No. PRG676), and the Estonian Energy Technology Program: SLOKT10209T "Nanomaterials – research and applications (NAMUR)" project 3.2.0304.12-0397. The author also thanks the private limited company AuVe Tech.

References

1. O. Z. Sharaf and M. F. Orhan, *Renew. sust. energ. rev.*, **32**, 810 (2014).
2. S. Sharma and B. G. Pollet, *J. Power Sources*, **208**, 96 (2012).
3. Y. Wang, K. S. Chen, J. Mishler, S. C. Cho, and X. C. Adroher, *Appl. Energ.*, **88**, 981 (2011).
4. Y.-J. Wang, B. Fang, H. Li, X. T. Bi, and H. Wang, *Prog. Mater. Sci.*, **82**, 445 (2016).
5. A. Adamson, R. Väli, M. Paalo, J. Aruväli, M. Koppel, R. Palm, E. Härk, J. Nerut, T. Romann, E. Lust, and A. Jänes, *RSC Adv.*, **10**, 20145 (2020).
6. E. Lust, K. Vaarmets, J. Nerut, I. Tallo, P. Valk, S. Sepp, and E. Härk, *Electrochim. Acta*, **140**, 294 (2014).
7. P. Valk, J. Nerut, R. Kanarbik, I. Tallo, J. Aruväli, and E. Lust, *J. Electrochem. Soc.*, **165**, F315 (2018).
8. M. Koppel, Gas sorption analysis of Mo2C derived carbon materials and quasi-elastic neutron scattering study of hydrogen diffusion, University of Tartu (2019) https://dspace.ut.ee/handle/10062/64720 (assessed 14 March 2022).
9. S. Sepp, K. Vaarmets, J. Nerut, I. Tallo, E. Tee, H. Kurig, J. Aruväli, R. Kanarbik, and E. Lust, *Electrochim. Acta*, **21**, 1035 (2017).
10. M. B. Sassin, Y. Garsany, B. D. Gould, and K. E. Swider-Lyons, *Anal. Chem.*, **89**, 511 (2017).
11. Microtrac Inc., Particle size analyzer manual, https://eng.auburn.edu/files/acad_depts/matl/lab-manuels/261%20-%20Analytical%20Lab/manuals/particle-size-analyzer-manual.pdf (assessed 14 March 2022).
12. S. Sepp, K. Vaarmets, J. Nerut, I. Tallo, E. Tee, H. Kurig, J. Aruväli, R. Kanarbik, and E. Lust, *Electrochim. Acta*, **203**, 221 (2016).
13. M. Härmas, R. Palm, T. Thomberg, R. Härmas, M. Koppel, M. Paalo, I. Tallo, T. Romann, A. Jänes, and E. Lust, *J Appl Electrochem*, **50**, 15 (2020).
14. J. W. Arblaster, *Platin. Met. Rev.*, **50**, 118 (2006).
15. I. N. Leontyev, A. B. Kuriganova, N. G. Leontyev, L. Hennet, A. Rakhmatullin, N. V. Smirnova, and V. Dmitriev, *RSC Adv.*, **4**, 35959 (2014).
16. S. Trasatti and O. A. Petrii, *J. Electroanal. Chem.*, **327**, 353 (1992).

Non-exclusive licence to reproduce the thesis and make the thesis public

I, Wiljar Lobjakas,

1. grant the University of Tartu a free permit (non-exclusive licence) to:

reproduce, for the purpose of preservation, including for adding to the DSpace digital archives until the expiry of the term of copyright, my thesis

„Platinum catalysts deposited onto peat-derived carbon for oxygen reduction reaction in a proton-exchange membrane fuel cell“,

supervised by Jaak Nerut and Heili Kasuk,

2. I grant the University of Tartu the permit to make the thesis specified in point 1 available to the public via the web environment of the University of Tartu, including via the DSpace digital archives, under the Creative Commons licence CC BY NC ND 4.0, which allows, by giving appropriate credit to the author, to reproduce, distribute the work and communicate it to the public, and prohibits the creation of derivative works and any commercial use of the work from ***01.06.2026*** until the expiry of the term of copyright,
3. I am aware that the author retains the rights specified in points 1 and 2.

4. I confirm that granting the non-exclusive licence does not infringe other persons' intellectual property rights or rights arising from the personal data protection legislation.

Wiljar Lobjakas
23.05.2023